Table 2 Clinical features of 18 patients with NIPC

Case no.	NIPC			ACE genotype	Primary disease	TBI/ TAI	GVHD		Donor		Alive or dead	Cause of death
	Diagnosis	Onset	Pattern of PFTs				Acute	Chronic [a]	Source	Relationship		
1	BOS	209	O	D/D	AML	+	II	E	BM	Unrelated	Dead	Respiratory failure
2	IP	172	R	D/D	MDS	+	0	U	BM	Unrelated	Dead	Respiratory failure
3	IP	164	N	D/D	AML	+	0	U	BM	Related	Alive	NA
4	IP	448	N	D/D	ALL	–	IV	E	PB	Related	Dead	Relapse
5	IPS	20	NE	D/D	ALL	+	III	NA	BM	Unrelated	Dead	Bacterial infection
6	IP	1331	M	I/D	AML	–	IV	E	PB	Related	Alive	NA
7	IP	518	R	D/D	AA	+	I	L	BM	Unrelated	Dead	Respiratory failure
8	BOOP	280	NE	D/D	NHL	+	I	E	BM	Unrelated	Dead	Respiratory failure
9	IP	210	R	I/I	NHL	–	II	E	PB	Related	Alive	NA
10	IP	604	O	D/D	AML	–	0	E	BM	Unrelated	Alive	NA
11	IP	170	R	D/D	MDS	–	0	E	PB	Related	Alive	NA
12	BOS	318	M	I/D	MDS	–	0	E	BM	Unrelated	Dead	Respiratory failure
13	IP	283	M	D/D	AML	–	0	U	PB	Related	Dead	Respiratory failure
14	IPS	25	O	D/D	AML	+	I	NA	PB	Related	Alive	NA
15	BOS	645	O	D/D	AA	+	III	L	BM	Unrelated	Alive	NA
16	BOS	381	O	I/I	MDS	–	I	L	PB	Related	Dead	Respiratory failure
17	IPS	130	NE	I/I	ATL	–	0	U	PB	Related	Dead	Respiratory failure
18	IP	190	R	I/D	ALL	+	III	U	PB	Related	Alive	NA

BOS bronchiolitis obliterans syndrome, *IP* interstitial pneumonia, *IPS* idiopathic pneumonia syndrome, *BOOP* bronchiolitis obliterans with organizing pneumonia, *PFTs* pulmonary function tests, *O* obstructive, *R* restrictive, *M* mixed, *N* normal, *NE* not examined, *D/D* deletion/deletion, *I/D* insertion/deletion, *I/I* insertion/insertion, *U* unremarkable, *L* limited, *E* extensive, *NA* not applicable, *BM* bone marrow, *PB* peripheral blood

[a] Severity of chronic GVHD before developing lung complication, excluding lung symptoms

categorization of NIPC was IP; $n = 10$, BOS; $n = 4$, IPS; $n = 3$, and bronchiolitis obliterans organizing pneumonia (BOOP); $n = 1$ (Table 2 and Supplemental Table 1). All patients were diagnosed basically according to their clinical features, because all patients have too serious pulmonary dysfunction to investigate lung biopsy. IP patients were diagnosed by their picture findings and restrictive pulmonary function test. BOS patients were diagnosed by obstructive pulmonary function test and absent the feature of infiltration lung picture. IPS and BOOP were diagnosed by clinical feature and picture studies. The mortality rate of NIPC was 44.4 % as a result of eight NIPC patients dying from respiratory failure (Table 2). The NIPC patient's clinical symptoms, results of PFTs, CT of the chest and chest radiograph findings are shown in Supplemental Table 1.

Clinical outcomes, *ACE* polymorphism, and developing NIPC

The distribution of *ACE* genotype reached statistical significance against the variables of donor source and regimen. The D/D genotype showed a significantly low frequency in CBT and RIST patients ($P = 0.048$ and $P = 0.038$, respectively) (Table 1). There was no significant association between *ACE* polymorphism and the other variables.

Two of the study patients died from graft failure before engraftment, thus these cases were treated as part of the competing event. Among the remaining 147 patients, aGVHD did not associate with developing NIPC ($P = 0.27$) (Table 3).

A total of 29 patients were omitted from the final analysis because of the following events that occurred

Table 3 The association with developing NIPC and GVHD

Variable	non-NIPC ($n = 131$)	NIPC ($n = 18$)	P	ACE genotype			P
				I/I	I/D	D/D	
aGVHD							
0–I	95	11		35	49	22	
II–IV	34	7	0.27	18	15	8	0.44
Competing[a]	2	0		1	0	1	
cGVHD[b]							
Limited-extensive	41	10		19	20	12	
Censored	63	6	0.11	22	35	12	0.46
Competing[c]	27	2		13	9	7	

[a] Two patients died before engraftment, so these patients were treated as part of the competing risk category to calculate this P value

[b] Chronic GVHD before developing NIPC

[c] Twenty-nine patients were died before 100 day. So, these cases treated as competing event

<100 days after transplantation: relapse, graft failure, developing NIPC, and death from any cause. Among the remaining 120 patients, 10/51 patients were diagnosed with chronic GVHD (cGVHD) and NIPC, and 6/69 patients were diagnosed with NIPC in the absence of cGVHD ($P = 0.11$) (Table 3). In this study, cGVHD and LONIPCs had no statistical association, so we analyzed the distribution of donor source and developing cGVHD. There was no association between the donor source and incidence of NIPC ($\chi^2 = 0.27$, $P = 0.60$).

The *ACE* polymorphism was not associated with aGVHD or cGVHD ($P = 0.44$ and $P = 0.46$, respectively), and did not significantly influence OS ($P = 0.91$) or the outcome of TRM and relapse (I/I + I/D: D/D; $P = 0.32$ and $P = 0.085$, respectively) (Fig. 2).

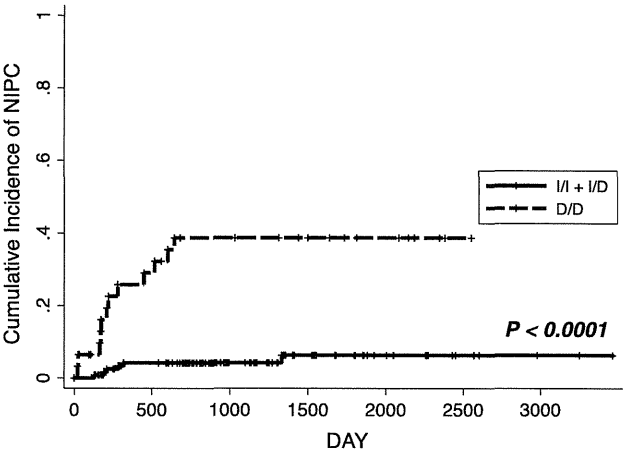

Fig. 2 Association of *ACE* polymorphism to clinical outcomes. **a** Cumulative incidence curve of transplantation-related mortality (TRM) among allogeneic HSCT patients comparing the *ACE* insertion genotypes and deletion polymorphisms (HR 1.53, $P = 0.32$, 95 % CI 0.7–3.5). **b** Cumulative incidence curve of relapse among 140 allogeneic HSCT patients diagnosed with malignant disease comparing the *ACE* insertion genotypes and deletion polymorphisms (HR 0.4, $P = 0.085$, 95 % CI 0.1–1.1)

ACE polymorphism and developing NIPC

A total of 31 patients in our cohort had the D/D genotype of the *ACE* polymorphism, and of these, 38.7 % (12/31) were diagnosed as NIPC, whereas I/D and I/I genotype patients represented 4.7 % (6/118). There was a significant difference in distribution pattern of the D/D, I/D, and I/I genotypes between NIPC patients and non-NIPC patients (HR 4.00, $P = 0.002$, 95 % CI 1.65–9.72), but there was no significant difference between I/D and I/I genotypes. Therefore, the D/D genotype was significantly more frequent in NIPC patients than in non-NIPC patients (HR 9.03, $P < 0.0001$, 95 % CI 3.4–24.2) (Fig. 3).

Multivariate analysis using a Fine and Gray model included *ACE* polymorphisms and PBSCT as criteria. This analysis identified the *ACE* D/D genotype as a significant factor impacting the development of NIPC (HR 8.8, $P < 0.0001$, 95 % CI 3.3–23.8) (Table 4).

Serum ACE levels in 116 subjects compared to *ACE* polymorphism

Of the 116 patients whose serum was available, 14 developed NIPC. The D/D genotype of *ACE* polymorphism was seen in 24 out of 116 patients and the frequency was not different from that among the 149 patients ($P = 1.00$). The mean serum ACE levels were significantly different among the three genotypes. Mean ACE levels and 95 % CIs were 10.44 (9.39–11.49), 12.49 (11.51–13.48) and 13.61 (11.86–15.37) IU/L (I/I, I/D, and D/D), respectively. The I/I genotype was associated with a significantly lower serum

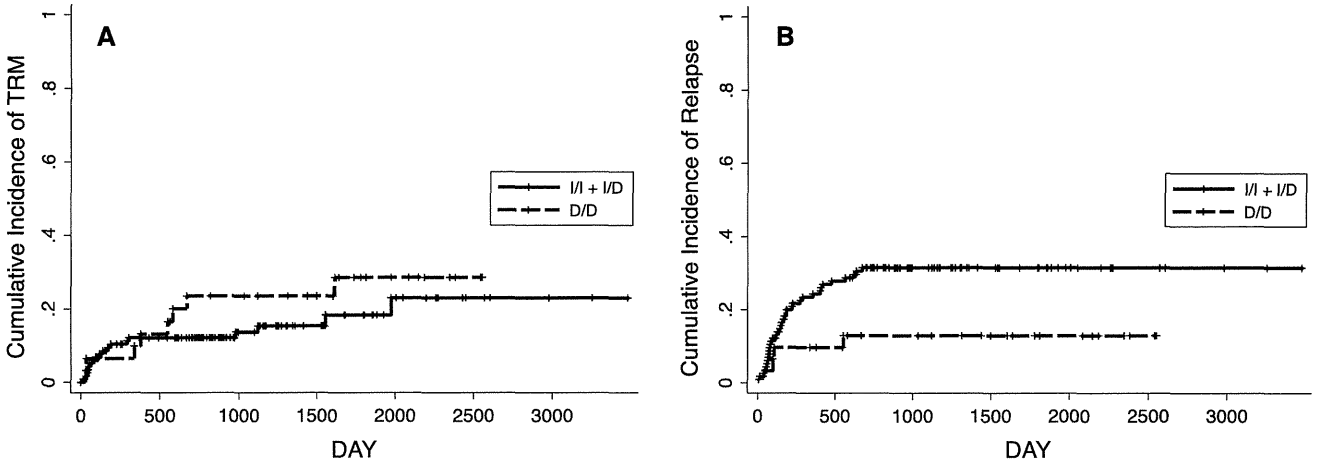

Fig. 3 NIPC and *ACE* polymorphisms. Cumulative incidence curve of NIPC among allogeneic HSCT patients comparing the *ACE* insertion genotypes and deletion polymorphisms (HR 9.03, $P < 0.0001$, 95 % CI 3.4–24.2)

Table 4 Competing risks regression test for development of NIPC

Variable	Hazard ratio (95 % CI)	*P*
ACE polymorphism		
I/D and I/I	1	
D/D	8.8 (3.8–23.8)	<0.0001
Donor source[a]		
BMT and CBT	1	
PBSCT	3.2 (0.6–18.3)	0.19

BMT bone marrow transplantation, *CBT* cord blood transplantation, *PBSCT* peripheral blood stem cell transplantation

[a] Considering the donor source, CBT also reached the selection criteria of multivariate factors, but CBT patients did not develop such an event in this study. So, CBT could not be treated as a factor in the time-to-event analysis. Thus, we calculated the donor source as PBSCT vs. BMT + CBT in this analysis

ACE level than the D/D genotype or I/D genotype (I/I vs. D/D; $P = 0.0006$ and I/I vs. I/D; $P = 0.0025$) (Fig. 4). However, we did not observe differences in serum ACE levels between NIPC and non-NIPC patients ($P = 0.38$).

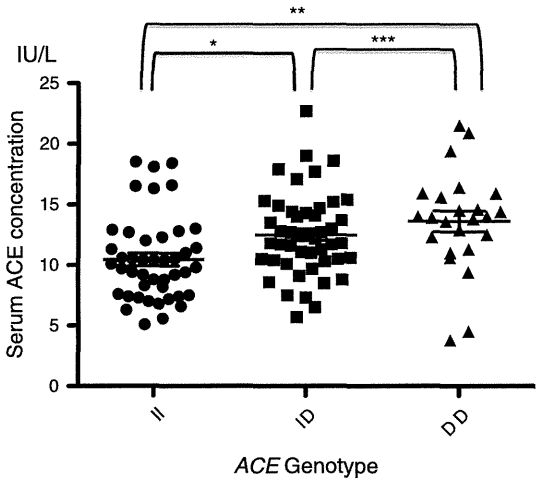

Fig. 4 Serum concentration of ACE and *ACE* polymorphisms in 116 subjects. The serum ACE levels differed significantly according to the *ACE* insertion/deletion polymorphism. (Student's *t* test, $*P = 0.0025$, $**P = 0.0006$ and $***P = 0.11$)

Discussion

Studies into the pathogenesis of lung injury after allogeneic HSCT using murine models revealed that inflammatory cytokines and lipopolysaccharide (LPS) are significant contributors to IPS pathogenesis [25–27]. Donor-derived cellular effectors are also recruited to the lung by specific receptor–ligand interactions that allow their passage through an inflamed pulmonary vascular endothelium and into the parenchyma, where they contribute to epithelial damage and dysfunction. However, there are no human studies to support these mechanisms derived from animal models.

This study supported the association between *ACE* deletion/insertion polymorphisms and NIPC in two independent patient cohorts. Our previous cohort was composed of patients who received HSCT from HLA-matched sibling donors [18], whereas the second cohort analyzed in the present study was comprised patients who received HSCT from both related and non-related donors. In spite of these differences in patient background, the presence of *ACE* deletion/insertion polymorphisms was the only common factor associated with NIPC in both univariate and multivariate analyses. Together, the results strongly implicate the renin-angiotensin system in a critical role in NIPC pathogenesis, supporting similar previous results in animal models.

ACE is a dipeptidyl carboxypeptidase that plays an important role in blood pressure regulation and electrolyte

balance by hydrolyzing angiotensin I to angiotensin II (A-II), which is a potent vasopressor and aldosterone-stimulating peptide. The *ACE* gene contains 26 exons and spans 21 kb located on chromosome 17q23. A-II plays a well-described role in the control of systemic blood pressure and volume homeostasis. A-II has also been implicated in the fibrotic response to tissue injury. Murine fibroblasts are stimulated to proliferate in the lung fibrotic response by angiotensin II, which is mediated by the AT1 receptor, and leads to lung fibrosis [10, 11, 13, 14]. *ACE* insertion/deletion polymorphisms are strongly associated with the level of the circulating ACE enzyme [17]. The mean plasma ACE level of D/D subjects is approximately twice that of I/I subjects, with I/D subjects having intermediate levels [16]. One clinical report also showed an association between pulmonary fibrosis and the *ACE* I/D polymorphism [15]. In allo-HSCT, several factors induce lung injury including the conditioning regimen, allo-reaction, and infection. Therefore, it is reasonable to suppose that higher plasma ACE may contribute to lung fibrosis and lead to NIPC.

Whereas the median onset of NIPC was 186 days in the former cohort, it was 245 days after transplantation in the present cohort. This includes only two patients with early onset of IPS and most with LONIPCs. Although previous studies have reported acute GVHD, high age of recipient, conventional conditioning, high dose of TBI, and high-risk disease [4, 5] as risk factors of IPS and LONIPCs, our analysis did not reach the statistical significance in analyzing these factors. Indeed, PBSCT was the only independent risk factor by univariate analysis. PBSCT and cGVHD were found to be associated with developing BOS in a recent multi-institute, retrospective analysis of 57 BOS patients out of 2087 HSCT recipients in Japan [28]. This study also reported that 5 out of 197 CBT cases developed BOS. Dudek et al. [29] reported that of 58 patients undergoing CBT, none developed BOS. In our study, CBT patients did not develop NIPC, but did show significantly low frequency of the *ACE* D/D genotype, which was associated with the highest risk for NIPC in our study (Table 1). However, the D/D genotype frequency was also significantly low among the RIST patients, and the conditioning regimen was not identified as a risk factor for NIPC by univariate or multivariate analysis. These findings may suggest that the donor source also influences the development of NIPC as in the case of GVHD. A further study is required to clarify the association since the sample size is too small in this study.

The association was confirmed between the *ACE* I/D polymorphism and serum ACE levels, as previously reported [17]. Although serum ACE levels at the pre-transplantation period did not predict NIPC development, patients with a high-risk genetic background and suffering from over-exposure to lung toxicity could develop NIPC. Even though both cohorts were analyzed in the present study we did not have enough statistical power to detect the previously reported risk factors such as cGVHD, but we demonstrated a strong association between the *ACE* I/D polymorphism and NIPC in both studies.

There is no standardized approach for the treatment of NIPC occurring after HSCT. This study revealed that the *ACE* D/D genotype is an independent risk factor for developing NIPC, and particularly the early onset IPS category. Interestingly, ACE inhibitors have shown success as blocking agents in experimental models of lung fibrosis [30, 31]. Lovastatin can induce apoptosis in normal and fibrotic lung fibroblasts in vitro [32]. Lovastatin has also been observed to reduce granulation tissue in association with ultrastructural evidence for fibroblast apoptosis in vivo using a guinea pig wound chamber model [32]. One retrospective analysis reported that 12 % of 478 patients with idiopathic pulmonary fibrosis (IPF) received an ACE inhibitor and no significant differences were observed in overall survival between the populations [33]. It should be considered that the expected effect of ACE inhibitors would be in preventing rather than resolving IPF. No randomized clinical studies have been published that assess the clinical relevance of ACE inhibitors or AT1 receptor antagonists in affecting IPF and/or NIPC after HSCT. Patients receiving HSCT are an ideal population for a prospective study of the use of these agents to prevent NIPC, because around 20 % of HSCT recipients develop NIPC as a complication of HSCT. We propose to undertake such a prospective study.

Acknowledgments This work was supported by the Research on Allergic Disease and Immunology (Health and Labor Science Research Grant H20-014, H23-010) from the Ministry of Health, Labor, and Welfare of Japan. We thank the laboratory staff at the Department of Hematology and Oncology at Tokai University for their kind support, especially Ms. Ito, Ms. Matsushita and Ms. Sekiya for supporting the genotyping work.

Conflict of interest None of the authors have any conflicts of interest to declare.

References

1. Clark JG, Hansen JA, Hertz MI, Parkman R, Jensen L, Peavy HH. Idiopathic pneumonia syndrome after bone-marrow transplantation. Am Rev Respir Dis. 1993;147:1601–6.
2. Panoskaltsis-Mortari A, Griese M, Madtes DK, et al. An official American thoracic society research statement: noninfectious lung injury after hematopoietic stem cell transplantation: idiopathic pneumonia syndrome. Am J Respir Crit Care Med. 2011;183:1262–79.
3. Cooke KR, Yanik G. Acute lung injury after allogeneic stem cell transplantation: is the lung a target of acute graft-versus-host disease? Bone Marrow Transplant. 2004;34:753–65.

4. Fukuda T, Hackman RC, Guthrie KA, et al. Risks and outcomes of idiopathic pneumonia syndrome after nonmyeloablative and conventional conditioning regimens for allogeneic hematopoietic stem cell transplantation. Blood. 2003;102:2777–85.
5. Sakaida E, Nakaseko C, Harima A, et al. Late-onset noninfectious pulmonary complications after allogeneic stem cell transplantation are significantly associated with chronic graft-versus-host disease and with the graft-versus-leukemia effect. Blood. 2003;102:4236–42.
6. Yanik G, Hellerstedt B, Custer J, et al. Etanercept (Enbrel) administration for idiopathic pneumonia syndrome after allogeneic hematopoietic stem cell transplantation. Biol Blood Marrow Transplant. 2002;8:395–400.
7. Palmas A, Tefferi A, Myers JL, et al. Late-onset noninfectious pulmonary complications after allogeneic bone marrow transplantation. Br J Haematol. 1998;100:680–7.
8. Afessa B, Litzow MR, Tefferi A. Bronchiolitis obliterans and other late onset non-infectious pulmonary complications in hematopoietic stem cell transplantation. Bone Marrow Transplant. 2001;28:425.
9. Patriarca F, Skert C, Sperotto A, et al. Incidence, outcome, and risk factors of late-onset noninfectious pulmonary complications after unrelated donor stem cell transplantation. Bone Marrow Transplant. 2004;33:751–8.
10. Uhal BD, Gidea C, Bargout R, et al. Captopril inhibits apoptosis in human lung epithelial cells: a potential antifibrotic mechanism. Am J Physiol Lung Cell Mol Physiol. 1998;275:L1013–7.
11. Wang R, Ramos C, Joshi I, et al. Human lung myofibroblast-derived inducers of alveolar epithelial apoptosis identified as angiotensin peptides. Am J Physiol Lung Cell Mol Physiol. 1999;277:L1158–64.
12. Wang R, Zagariya A, Ang E, Ibarra-Sunga O, Uhal BD. Fas-induced apoptosis of alveolar epithelial cells requires ANG II generation and receptor interaction. Am J Physiol Lung Cell Mol Physiol. 1999;277:L1245–50.
13. Marshall RP, McAnulty RJ, Laurent GJ. Angiotensin II is mitogenic for human lung fibroblasts via activation of the type 1 receptor. Am J Respir Crit Care Med. 2000;161:1999–2004.
14. Marshall RP, Gohlke P, Chambers RC, et al. Angiotensin II and the fibroproliferative response to acute lung injury. Am J Physiol Lung Cell Mol Physiol. 2004;286:L156–64.
15. Morrison CD, Papp AC, Hejmanowski AQ, Addis VM, Prior TW. Increased D allele frequency of the angiotensin-converting enzyme gene in pulmonary fibrosis. Hum Pathol. 2001;32:521–8.
16. Rigat B, Hubert C, Alhenc-Gelas F, Cambien F, Corvol P, Soubrier F. An insertion/deletion polymorphism in the angiotensin I-converting enzyme gene accounting for half the variance of serum enzyme levels. J Clin Invest. 1990;86:1343–6.
17. Tiret L, Rigat B, Visvikis S, et al. Evidence, from combined segregation and linkage analysis, that a variant of the angiotensin I-converting enzyme (ACE) gene controls plasma ACE levels. Am J Hum Genet. 1992;51:197–205.
18. Onizuka M, Kasai M, Oba T, et al. Increased frequency of the angiotensin-converting enzyme gene D-allele is associated with noninfectious pulmonary dysfunction following allogeneic stem cell transplant. Bone Marrow Transplant. 2005;36:617–20.
19. Sorror ML, Maris MB, Storb R, et al. Hematopoietic cell transplantation (HCT)-specific comorbidity index: a new tool for risk assessment before allogeneic HCT. Blood. 2005;106:2912–9.
20. Higaki J, Baba S, Katsuya T, et al. Deletion allele of angiotensin-converting enzyme gene increases risk of essential hypertension in Japanese men: the Suita study. Circulation. 2000;101:2060–5.
21. Ascioglu S, Rex JH, de Pauw B, et al. Defining opportunistic invasive fungal infections in immunocompromised patients with cancer and hematopoietic stem cell transplants: an international consensus. Clin Infect Dis. 2002;34:7–14.
22. Chien JW, Duncan S, Williams KM, Pavletic SZ. Bronchiolitis obliterans syndrome after allogeneic hematopoietic stem cell transplantation—an increasingly recognized manifestation of chronic graft-versus-host disease. Biol Blood Marrow Transpl. 2010;16:S106–14.
23. Yoshihara S, Yanik G, Cooke KR, Mineishi S. Bronchiolitis obliterans syndrome (BOS), bronchiolitis obliterans organizing pneumonia (BOOP), and other late-onset noninfectious pulmonary complications following allogeneic hematopoietic stem cell transplantation. Biol Blood Marrow Transpl. 2007;13:749–59.
24. Fine JPGR. A proportional hazards model for the sub distribution of a competing risk. J Am Stat Assoc. 1999;94:496–509.
25. Cooke KR, Hill GR, Crawford JM, et al. Tumor necrosis factor-alpha production to lipopolysaccharide stimulation by donor cells predicts the severity of experimental acute graft-versus-host disease. J Clin Invest. 1998;102:1882–91.
26. Cooke KR, Kobzik L, Martin TR, et al. An experimental model of idiopathic pneumonia syndrome after bone marrow transplantation: I. The roles of minor H antigens and endotoxin. Blood. 1996;88:3230–9.
27. Cooke KR, Krenger W, Hill G, et al. Host reactive donor T cells are associated with lung injury after experimental allogeneic bone marrow transplantation. Blood. 1998;92:2571–80.
28. Nakaseko C, Ozawa S, Sakaida E, et al. Incidence, risk factors and outcomes of bronchiolitis obliterans after allogeneic stem cell transplantation. Int J Hematol. 2011;93:375–82.
29. Dudek AZ, Mahaseth H, DeFor TE, Weisdorf DJ. Bronchiolitis obliterans in chronic graft-versus-host disease: analysis of risk factors and treatment outcomes. Biol Blood Marrow Transpl. 2003;9:657–66.
30. Wang R, Ibarra-Sunga O, Verlinski L, Pick R, Uhal BD. Abrogation of bleomycin-induced epithelial apoptosis and lung fibrosis by captopril or by a caspase inhibitor. Am J Physiol Lung Cell Mol Physiol. 2000;279:L143–51.
31. Molteni A, Moulder JE, Cohen EF, et al. Control of radiation-induced pneumopathy and lung fibrosis by angiotensin-converting enzyme inhibitors and an angiotensin II type 1 receptor blocker. Int J Radiat Biol. 2000;76:523–32.
32. Tan A, Levrey H, Dahm C, Polunovsky VA, Rubins J, Bitterman PB. Lovastatin induces fibroblast apoptosis in vitro and in vivo. Am J Respir Crit Care Med. 1999;159:220–7.
33. Nadrous HF, Ryu JH, Douglas WW, Decker PA, Olson EJ. Impact of angiotensin-converting enzyme inhibitors and statins on survival in idiopathic pulmonary fibrosis*. CHEST J. 2004;126:438–46.

Generation of Engraftable Hematopoietic Stem Cells From Induced Pluripotent Stem Cells by Way of Teratoma Formation

Nao Suzuki[1,2], Satoshi Yamazaki[1,3], Tomoyuki Yamaguchi[1,3], Motohito Okabe[1], Hideki Masaki[3], Satoshi Takaki[2], Makoto Otsu[1] and Hiromitsu Nakauchi[1,3]

[1]Division of Stem Cell Therapy, Center for Stem Cell Biology and Regenerative Medicine, Institute of Medical Science, University of Tokyo, Tokyo, Japan; [2]Department of Immune Regulation Research Institute, National Center for Global Health and Medicine, Chiba, Japan; [3]Japan Science Technology Agency, Exploratory Research for Advanced Technology (ERATO) Nakauchi Stem Cell and Organ Regeneration Project, Tokyo, Japan

In vitro generation of hematopoietic stem cells (HSCs) from induced pluripotent stem cells (iPSCs) has the potential to provide novel therapeutic approaches for replacing bone marrow (BM) transplantation without rejection or graft versus host disease. Hitherto, however, it has proved difficult to generate truly functional HSCs transplantable to adult host mice. Here, we demonstrate a unique *in vivo* differentiation system yielding engraftable HSCs from mouse and human iPSCs in teratoma-bearing animals in combination with a maneuver to facilitate hematopoiesis. In mice, we found that iPSC-derived HSCs migrate from teratomas into the BM and their intravenous injection into irradiated recipients resulted in multilineage and long-term reconstitution of the hematolymphopoietic system in serial transfers. Using this *in vivo* generation system, we could demonstrate that X-linked severe combined immunodeficiency (X-SCID) mice can be treated by HSCs derived from gene-corrected clonal iPSCs. It should also be noted that neither leukemia nor tumors were observed in recipients after transplantation of iPSC-derived HSCs. Taken our findings together, our system presented in this report should provide a useful tool not only for the study of HSCs, but also for practical application of iPSCs in the treatment of hematologic and immunologic diseases.

Received 6 January 2013; accepted 17 March 2013; advance online publication 14 May 2013. doi:10.1038/mt.2013.71

INTRODUCTION

Direct reprogramming of somatic cells allows generation of patient-specific induced pluripotent stem cell (iPSC) lines similar to embryonic stem cells (ESCs).[1–3] Such iPSCs are capable of self-renewal, large-scale expansion, and differentiation into all three germ layers, opening a way to cell therapy using a patient's own cells.[4–6] For instance, when iPSCs are propagated and gene-corrected *in vitro*, hematopoietic stem cells (HSCs) derived from them can be transplanted, as curative therapy, into patients with genetic hematologic disorders. Efficient differentiation of iPSCs into functional HSCs is the most important goal for future HSC-based cell or gene therapies. Although *in vitro* generation of HSCs from mouse ESCs through forced expression of *HOXB4* has been reported, the resultant HSCs exhibited abnormal hematopoiesis.[7,8] Furthermore, forced expression of *HOXB4* is not helpful in generating human HSCs.[9] Generation of fully functional HSCs from mouse or human iPSCs without any genetic modifications has rarely been accomplished.[10,11] One of the reasons is that it is difficult to reproduce the microenvironment necessary for development of hematopoietic lineage cells during embryogenesis. In addition, recapitulation of an adult HSC niche *in vitro* has also been complicate by the fact that not all the cell types composing the HSC niche are known.

From these reasons, we considered use of teratomas as the differentiation site of hematopoietic lineage cells and engraftable HSCs from ESCs or iPSCs. Teratomas are benign tumors containing differentiated tissues of all three germ layers artificially formed by an injection of ESCs/iPSCs into immunodeficient mice. Erythrocytes, megakaryocytes, and blood vessels develop within teratomas formed in chickens or mice.[12–15] We hypothesized that a microenvironment like that in developing embryos, that allows generation of hematopoietic lineage cells, might be formed in teratomas and that functional iPSC-derived HSCs, once generated, would eventually migrate to the bone marrow (BM) niche just as bona fide HSCs behave *in vivo*[16,17] (**Figure 1a**).

Here, we established an *in vivo* differentiation system to generate fully functional HSCs from iPSCs through teratoma

The first two authors contributed equally to this work.

Correspondence: *Hiromitsu Nakauchi, Division of Stem Cell Therapy, Center for Stem Cell Biology and Regenerative Medicine, Japan Science Technology Agency, Exploratory Research for Advanced Technology (ERATO) Nakauchi Stem Cell and Organ Regeneration Project, 4-6-1 Shirokanedai, Minato-ku, Tokyo 108-8639, Japan. E-mail: nakauchi@ims.u-tokyo.ac.jp or Satoshi Yamazaki, Division of Stem Cell Therapy, Center for Stem Cell Biology and Regenerative Medicine, Japan Science Technology Agency, Exploratory Research for Advanced Technology (ERATO) Nakauchi Stem Cell and Organ Regeneration Project, 4-6-1 Shirokanedai, Minato-ku, Tokyo 108-8639, Japan. E-mail: y-sato4@imu.u-tokyo.ac.jp*

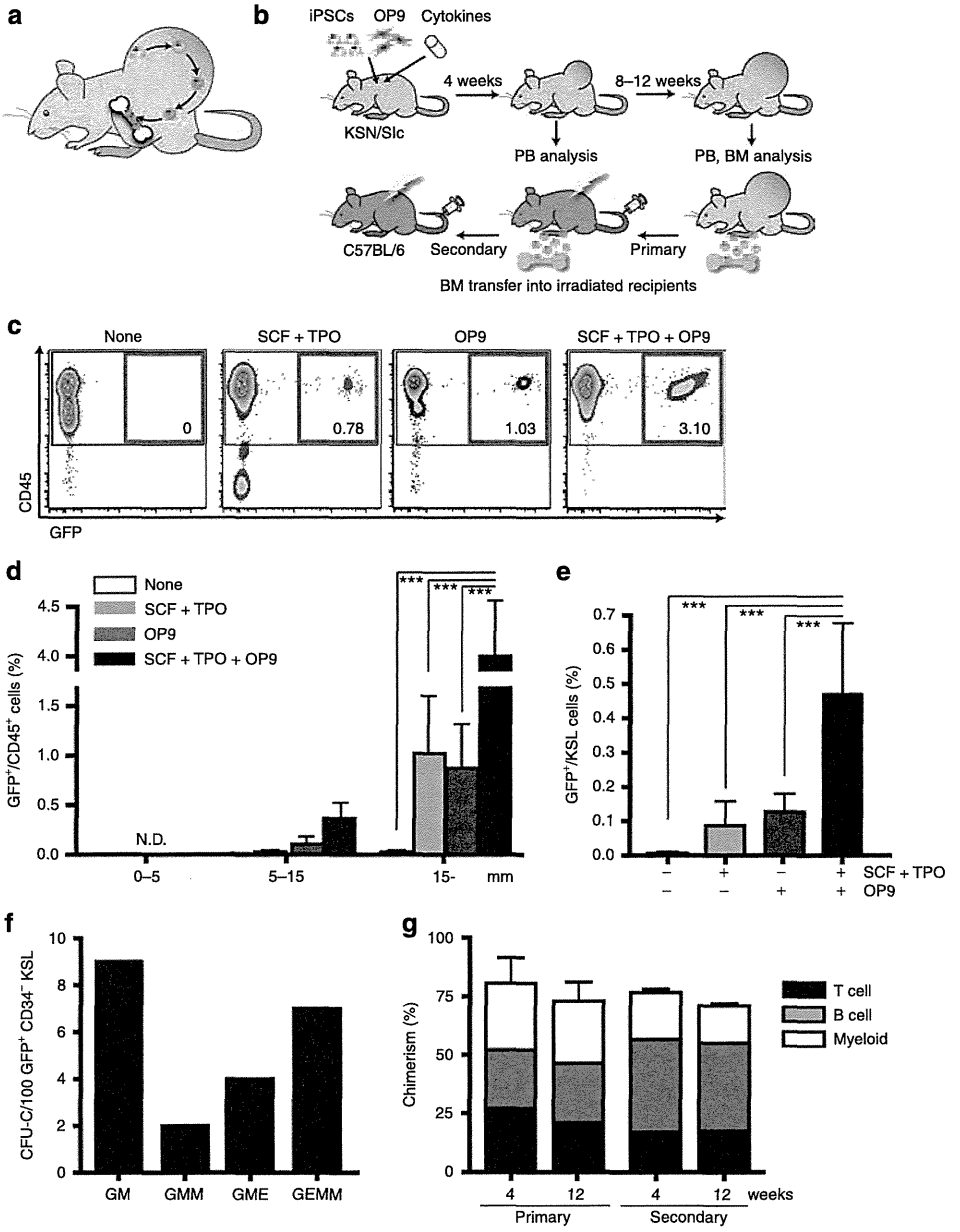

Figure 1 Generation of transplantable hematopoietic stem cells (HSCs) from LG-iPSCs through teratoma formation. (**a**) The hypothesized model for the homing of iPSC-derived HSCs from teratoma into bone marrow (BM). (**b**) Strategy to induce HSCs from iPSCs through teratoma formation. With or without OP9 cells, iPSCs were subcutaneously injected into nude mice. Cytokines were administered for 2 weeks using a micro-osmotic pump. BM cells, among which iPSC-derived HSCs were detectable, were transplanted into irradiated mice. (**c**) Flow cytometric analysis of peripheral blood (PB) in teratoma-bearing nude mice 12 weeks after iPSC injection. Numbers represent percentages of $GFP^+/CD45^+$ cells. (**d**) Time course change of $GFP^+/CD45^+$ cells in PB dependent on teratoma size. The *X*-axis represents teratoma size (***$P < 0.001$). (**e**) Percentages of GFP^+/KSL cells in BM of nude teratoma-bearing mice. Analysis conducted 12 weeks after iPSC injection ($n = 5$ per group). Error bars represent SEM (***$P < 0.001$). (**f**) Hundred GFP^+ $CD34^-$ KSL cells in BM of teratoma-bearing mice were single-cell sorted and cultured for 10 days with cytokines for hematopoietic differentiation. (**g**) BM transplantation assay for chimerism of LG-iPSC–derived $GFP^+/CD45^+$ cells in PB of recipient mice. BM cells of teratoma-bearing mice were transplanted into irradiated mice. Secondary transplantation was also performed 12 weeks after primary transplantation. (Primary, $n = 4$; secondary, $n = 10$.) Error bars represent SEM. CFU-C, colony-forming unit in culture; GFP, green fluorescent protein; GM, granulocyte macrophage; GMM, granulocyte macrophage megakaryocyte; GME, granulocyte macrophage erythroid; GEMM, granulocyte erythroblast macrophage megakaryocyte multilineage; LG-iPSC, *Lnk*$^{-/-}$ *GFP* transgenic mice-induced pluripotent stem cell; N.D., not detectable; SCF, stem cell factor; TPO, thrombopoietin.

formation. To monitor the system, we evaluated induction of HSCs with *Lnk*$^{-/-}$ iPSCs that have a high hematopoietic potential. We then successfully generated engraftable HSCs from mouse iPSCs without any genetic modifications. Moreover, we obtained a proof-of-concept for the next generation of gene therapy using iPSCs in an X-linked severe combined immunodeficiency (X-SCID) mouse model and also succeeded in inducing xenotransplantable HSCs from human iPSCs.

RESULTS

Generation of iPSC-derived transplantable HSCs in *Lnk*$^{-/-}$ mice through teratoma formation with combined administration of hematopoietic cytokines and stromal cells

According to our speculation that HSC induction from iPSCs derived from wild-type mice might be a very rare event, we chose to use iPSCs derived from *Lnk*$^{-/-}$ *GFP* transgenic mice (LG-iPSCs). Lnk is an intracellular adaptor protein reported to be a negative regulator of HSC self-renewal.[18] *Lnk*$^{-/-}$ mice overproduce HSCs[19] due to their extreme self-renewing capability;[20] thus once generated, we expected to be able to detect LG-iPSC–derived HSCs even when induction efficiency was very low. We first injected LG-iPSCs alone into KSN/Slc nude mice subcutaneously, but we were not able to detect donor-derived green fluorescent protein$^+$ (GFP$^+$) cells in the peripheral blood (PB) of teratoma-bearing mice. Co-culturing with OP9 stromal cells supplemented with stem cell factor (SCF) and thrombopoietin (TPO) has been used to induce hematopoietic progenitors from ESCs/iPSCs *in vitro*.[7] In an attempt to increase the efficiency of HSC induction, we co-injected LG-iPSCs with OP9 cells and subcutaneously implanted a micro-osmotic pump to supply hematopoietic cytokines (**Figure 1b**). After 8–10 weeks, LG-iPSC–derived GFP$^+$ CD45$^+$ cells appeared in PB of mice treated with cytokines, OP9 cells, or a combination of both (**Figure 1c**). The frequency of GFP$^+$ CD45$^+$ cells in PB gradually increased with teratoma enlargement (**Figure 1d** and **Supplementary Figure S1a**). Combined administration of cytokines and OP9 cells was most efficient for the production of GFP$^+$ CD45$^+$ cells (average values 12 weeks after iPSC injection: none, 0.002 ± 0.01%; SCF + TPO, 1.02 ± 1.15%; OP9, 0.87 ± 0.79%; SCF + TPO + OP9, 4.26 ± 3.79%) (**Figure 1d**). In the BM of teratoma-bearing mice 12 weeks after iPSC injection, GFP$^+$ cells could be detected among Lineage-negative (Lin$^-$) cells as multipotent progenitors, Lin$^-$ c-Kit$^+$ Sca-1$^+$ (KSL) cells as hematopoietic stem progenitor cells, and CD34$^-$ KSL cells as long-term HSCs (**Supplementary Figure S1b**). The frequency of LG-iPSC–derived KSL cells was highest when both cytokines and OP9 cells were administered, correlating with the frequency of circulating iPSC-derived CD45$^+$ cells in PB (**Figure 1e**). These data suggest that immunophenotypically defined HSCs, originating from LG-iPSCs and capable of homing to host BM through the blood circulation, were generated through teratoma formation and that the supplementation with hematopoietic cytokines and OP9 cells enhanced the process.

To test the function, GFP$^+$ CD34$^-$ KSL cells in BM of the teratoma-bearing mouse were sorted as single cells and individual cells were cultured for 10 days with cytokines for colony formation. Among the seeded CD34$^-$ KSL cells, 22.9% formed large colonies exhibiting colony-forming unit (CFU)-granurocyte/erythroblast/macrophage/megakaryocyte (GEMM) differentiation (data not shown), with evidence of robust multipotency at the clonal level, along with other types of colonies with more restricted differentiation properties (**Figure 1f**). To determine whether LG-iPSC–derived HSCs had any marrow-repopulating ability, 1×10^7 BM cells of teratoma-bearing mice were transplanted into lethally irradiated C57BL/6 (B6) mice as primary recipients. Sequential analysis of PB cells of recipient mice detected LG-iPSC–derived hematopoietic cells at high frequencies (4 weeks, 77.7 ± 18.9%; 12 weeks, 73.0 ± 16.5% mean ± SEM, $n = 4$ each) with multilineage reconstitution (**Figure 1g**, primary; **Supplementary Table S1**). LG-iPSC–derived cells were also detected in spleen and BM of recipient mice, with the average percentage of GFP$^+$ cells within CD34$^-$ KSL fractions as high as 45.0% (**Supplementary Figure S1c,d** and **Supplementary Table S1**). BM cells of these primary recipients (1×10^7 cells) were then serially transplanted into secondary recipients to test the self-renewal potential with LG-iPSC–derived HSCs. Multiple lineage reconstitution by LG-iPSC–derived cells in secondary recipient mice was observed for more than 12 weeks after transplantation (4 weeks, 76.6 ± 2.7%; 12 weeks, 60.6 ± 4.6% mean ± SEM, $n = 10$ each) (**Figure 1g**, secondary). These results demonstrated that HSCs with self-renewal and multilineage differentiation capabilities were generated from LG-iPSCs through teratoma formation.

Generation of functional HSCs from normal mouse iPSCs through teratoma formation

To determine whether functional HSCs can be induced from iPSCs without *Lnk* deficiency, we established iPSCs from B6 *GFP* transgenic mice (G-iPSCs) and assessed the generation of HSCs through teratoma formation. G-iPSC–derived hematopoietic cells, unlike LG-iPSCs, were rare but detectable in PB of teratoma-bearing mice, with the exception of those receiving G-iPSC alone (**Figure 2a** and **Supplementary Figure S2a**). The highest frequencies of GFP$^+$ CD45$^+$ cells were consistently observed in the presence of cytokines and OP9 cells (% GFP$^+$/CD45$^+$ cells: none, 0.003 ± 0.006%; SCF + TPO, 0.01 3 ± 0.01%; OP9, 0.025 ± 0.01%; SCF + TPO + OP9, 0.16 ± 0.09% mean ± SD, $n = 4$ each) (**Figure 2a**). GFP$^+$ cells were also detected among Lin$^-$ cells, KSL cells, and CD34$^-$ KSL cells in BM of teratoma-bearing mice at 12 weeks after iPSC injection (**Supplementary Figure S2b**). Using G-iPSC–derived CD34$^-$ KSL cells from BM of teratoma-bearing mice, we evaluated early multilineage differentiation. In the presence of cytokines for hematopoietic differentiation, we observed single G-iPSC–derived CFU-GEMM mixed colonies (**Figure 2b**). Transplantation of BM cells obtained from teratoma-bearing mice (1×10^7 cells) led to engraftment of G-iPSC–derived blood cells in PB, spleen, and BM of primary recipient mice (**Figure 2c**, primary; **Supplementary Figure S2c**). Chimerism in this experiment was much lower than when LG-iPSC–derived HSCs were transplanted (**Supplementary Table S1**), presumably because wild-type mouse iPSC-derived HSCs have lower capability for self-renewal and for homing to the host BM niche. GFP$^+$ cells were also detected in primitive hematopoietic fractions, including Lin$^-$ cells, KSL cells, and CD34$^-$ KSL cells within recipient BM (**Supplementary Figure S2d**). To examine the reconstitution activity of G-iPSC–derived HSCs, we transplanted 40 sorted GFP$^+$ CD34$^-$ KSL cells from primary recipients along with 2×10^5 B6 BM cells into secondary recipient mice. This transplantation led to robust engraftment of GFP$^+$ cells at multilineage levels, with chimerism maintained for between 4 and 12 weeks after transplantation (**Figure 2c**, secondary). These data suggest that our HSC induction system allows generation of engraftable HSCs even from iPSCs having no *Lnk* mutations. Leukemia and other abnormalities were not observed in any recipient mice in transplantation

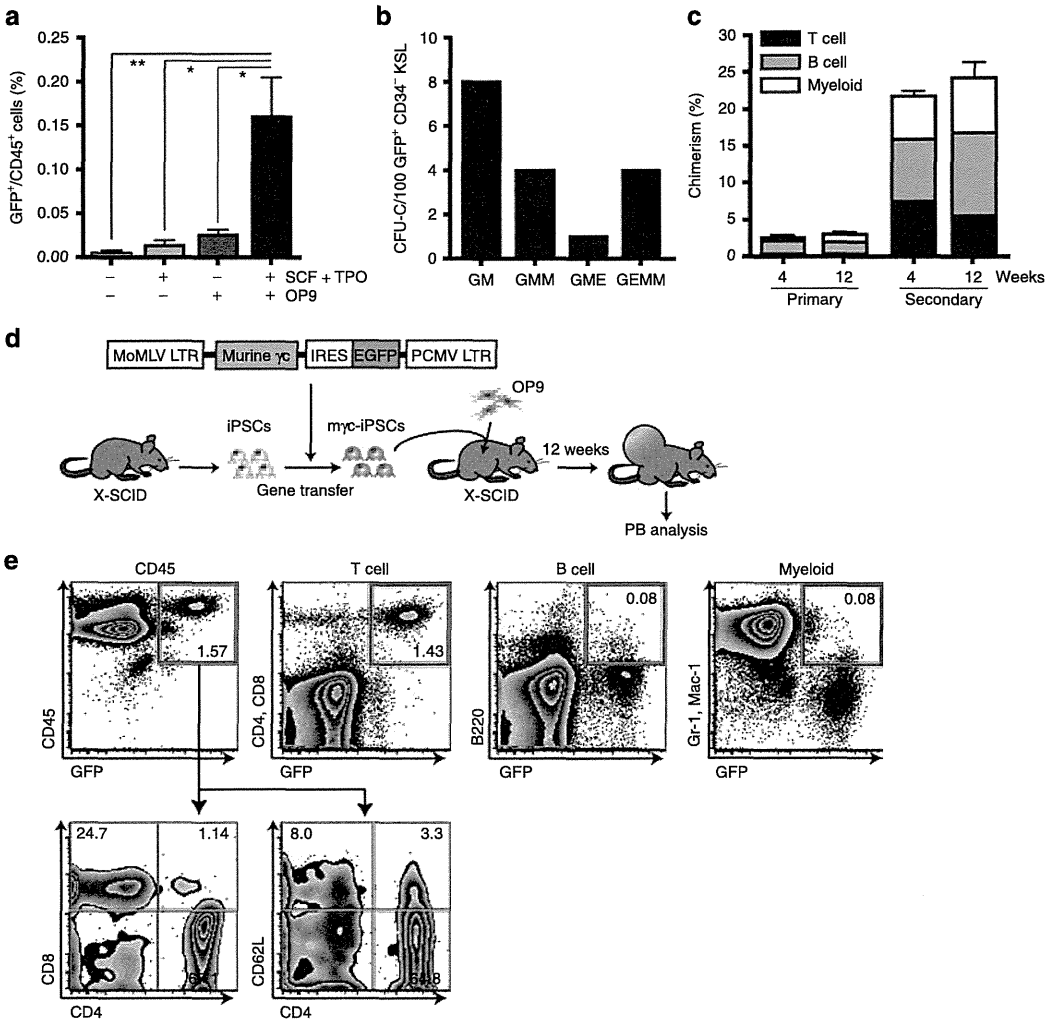

Figure 2 Generation of transplantable hematopoietic stem cells (HSCs) from G-iPSCs through teratoma formation, with the gene therapy model of X-SCID. (**a**) Percentages of $GFP^+/CD45^+$ cells in peripheral blood (PB) of nude teratoma-bearing mice. Analysis was conducted 12 weeks after iPSC injection ($n = 4$ per group). Error bars represent SD (*$P < 0.05$, **$P < 0.01$). (**b**) Hundred GFP^+ $CD34^-$ KSL cells in bone marrow (BM) of teratoma-bearing mice were single-cell sorted and cultured with cytokines for hematopoietic differentiation. Numbers and types of CFC-GEMM were evaluated on day 10. (**c**) BM transplantation assay for chimerism of G-iPSC–derived GFP^+ hematopoietic cells/$CD45^+$ cells in PB of recipient mice. Whole BM cells of teratoma-bearing mice were transplanted into primary recipient mice. Forty FACS-sorted GFP^+ $CD34^-$ KSL cells in BM of primary recipient mouse were transplanted into secondary recipient mice. (Primary, $n = 6$; secondary, $n = 5$.). Error bars represent SD. (**d**) Flow chart explaining the generation of T cells from mγc-iPSCs in X-SCID mice. iPSCs were established from X-SCID mice and mγc was transduced, yielding mγc-iPSCs. mγc-iPSCs and OP9 cells were injected into X-SCID mice to generate teratomas. (**e**) Flow cytometric analysis of PB in teratoma-bearing mice 12 weeks after iPSC injection. Numbers represent percentages. CFC-GEMM, colony-forming cell-granulocyte erythroblast macrophage megakaryocyte multilineage; EGFP, enhanced green fluorescent protein; FACS, fluorescence-activated cell sorting; G-iPSC, *GFP* transgenic mice-induced pluripotent stem cell; IRES, internal ribosomal entry site; LTR, long terminal repeat; SCF, stem cell factor; TPO, thrombopoietin; X-SCID, X-linked severe combined immunodeficiency.

experiments (**Supplementary Figure S2e**), implying that induced HSCs have normal hematopoietic properties.

Reconstitution of lymphocytes in X-SCID mice by HSCs derived from gene-corrected clonal X-SCID-iPSCs

To validate the utility of our HSCs induction system in principle, we established a therapeutic model for X-SCID utilizing gene correction of disease-specific iPSCs. X-SCID causes severely impaired T and B cell immunity[21] due to a mutation in the gene encoding the common gamma chain (γc), whose product is shared by receptors for multiple immunologically important cytokines. Stem cell gene therapy is effective in X-SCID, but its use has multiple risks.[22,23] While gene therapy utilizing clonal disease-specific iPSCs screened for safety[24] may be a solution, generation of genuine HSCs has been a major obstacle. We first generated iPSCs from X-SCID mice, and then established a clonal cell line expressing murine γc (mγc-iPSCs) by retroviral gene transfer (**Figure 2d** and **Supplementary Figure S3**). We then subcutaneously injected mγc-iPSCs into X-SCID mice with OP9 cells to generate teratomas. Twelve weeks after iPSC injection, mature T cells derived from functionally corrected mγc-iPSCs were clearly observed with normal distributions of $CD4^+$ or $CD8^+$ cells and evidence of naive T cell ($CD4^+$ $CD62L^+$) generation in PB

of teratoma-bearing X-SCID mice (**Figure 2e**). Only trace levels of B- and myeloid-lineage cells expressing GFP appeared, likely due to competition with their residual counterparts in host BM. These results proved that, in principle, the immunodeficiency of X-SCID can be treated by HSCs generated from gene-corrected iPSC-derived teratomas.

Production of HSCs with BM reconstitution potential from human iPSCs

Then, to investigate whether functional HSCs could also be induced from human iPSCs, we injected human iPSCs into testes of NOD/SCID mice to generate teratomas and, with them, HSCs. The frequencies of iPSC-derived cells were then analyzed in PB and BM of teratoma-bearing mice after 12 weeks (**Figure 3a**). PB of two mice among 15 contained a detectable mCD45$^-$ hCD45$^+$ cell population (**Figure 3b**, left panel and **Supplementary Figure S4a**). Furthermore, we could detect hCD45^{dull} hCD34$^+$ cells (a highly enriched human HSC population) and hCD45$^+$ hCD34$^-$ cells (terminally differentiated blood cells) within a mCD45-negative population in BM of 11 of 15 teratoma-bearing mice (**Figure 3b**, right panel and **Supplementary Figure S4a**). These findings demonstrated that human iPSC-derived hematopoietic cells can be generated *via* teratoma formation, and that they circulate through xenogenic mouse PB and BM. Then, we evaluated the multilineage differentiation capacity of human iPSC-derived HSCs using colony assay and observed typical morphology of various subtypes including CFU-GEMM (**Figure 3c**). A previous study revealed that human ESC-derived erythroid-like cells coexpress high levels of embryonic and fetal globins, but no adult globins.[25] We therefore examined expression of different globins in human iPSC-derived CFU-erythroid colonies. As a result, we could detect expression of all types in human iPSC-derived CFU-erythroid colonies as well as in cord blood-derived CFU-erythroid colonies, but no embryonic Hb Gower-1 ($\zeta_2\varepsilon_2$) expression in human PB (**Figure 3d**). These data suggest that erythrocytes expressing adult type Hb-A ($\alpha_2\beta_2$) were induced in iPSC-derived CFU-erythroid colonies, although cells expressing embryonic Hb Gower-1 and fetal Hb-F ($\alpha_2\gamma_2$), and adult Hb-A co-existed in iPSC-derived colonies as well as cord blood-derived colonies due to *in vitro* differentiation. To confirm the repopulating ability of human iPSC-derived HSCs, we transplanted mCD45$^-$ hCD45$^+$ hCD34$^+$ BM cells (600 cells) obtained from teratoma-bearing mice into irradiated NOD/SCID or NOD/SCID/JAK3^{null} mice (**Figure 3a**). This resulted in engraftment of human iPSC-derived blood cells with a multilineage repopulation including hGlycophorinA$^+$ erythrocytes and hCD3$^+$ T cells in PB of some recipient mice at 12 weeks after transplantation (**Figure 3e** and **Supplementary Figure S4b–g**). A higher proportion of engrafted mice was observed in NOD/SCID/JAK3^{null} recipient mice (29.4%) than in NOD/SCID recipient mice (3.57%) (**Supplementary Figure S4a**). Our findings established that engraftable HSCs which could differentiate into all hematopoietic lineages had been induced from human iPSCs without any genetic modifications.

HSC niche-like cells exist in iPSC-derived teratomas

Finally, to study how iPSC-derived blood cells or HSCs are generated and ascertain whether they might exist in teratomas, we analyzed

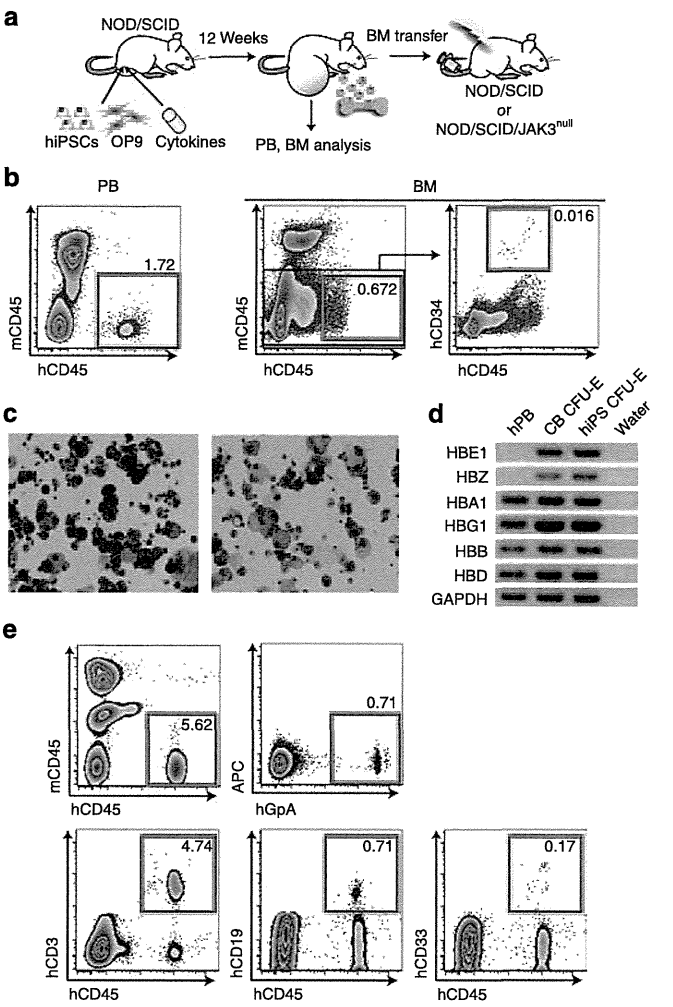

Figure 3 Induction of engraftable hematopoietic stem cells (HSCs) from human iPSCs through teratoma formation. (**a**) Strategy to induce HSCs from human induced pluripotent stem cells (iPSCs) through teratoma formation. iPSCs were injected with OP9 cells into testes of NOD/SCID mice. Cytokines were administered for 2 weeks *via* a micro-osmotic pump. BM cells of teratoma-bearing mice were transplanted into sublethally (3 Gy) irradiated NOD/SCID or NOD/SCID/JAK3^{null} mice. (**b**) Flow cytometric analysis of PB (left panel) and BM cells (right panels) in teratoma-bearing mice 12 weeks after human iPSC (hiPSC) injection. (**c**,**d**) Colony-forming assay with human iPSC-derived hCD45^{dull} hCD34$^+$ HSCs isolated from BM of teratoma-bearing mice. (**c**) Wright-Giemsa staining of cytospin preparations of CFU-GEMM mixed colonies. (**d**) Reverse transcription-PCR analysis for the expression of embryonic, fetal, and adult globins in cells taken from CFU-E colonies derived from human iPSCs. Human (h) PB cDNA was used as positive control. CB-derived CFU-E cDNA was used as control. Water is the negative control. HBE1: ε chain, HBZ: ζ chain, HBA1: α chain, HBG1: γ chain, HBB: β chain, and HBD: δ chain. (**e**) mCD45$^-$ hCD45$^+$ hCD34$^+$ 600 cells in BM of teratoma-bearing NOD/SCID mice were transplanted into irradiated NOD/SCID/JAK3^{null} mice with 2×10^5 NOD/SCID/JAK3^{null} BM cells. PB chimerism in recipient mice 12 weeks after BM transplantation. APC, allophycocyanin; BM, bone marrow; CB, cord blood; CFU-E, colony-forming unit-erythroid; PB, peripheral blood; SCID, severe combined immunodeficiency.

cells composing G-iPSC–derived teratomas formed in experimental mice. In addition to GFP$^+$ CD45$^+$ hematopoietic cells, GFP$^-$ CD45$^+$ cells were detected by immunostaining at 12 weeks after iPSC injection (**Figure 4a**). These cells were thought to infiltrate

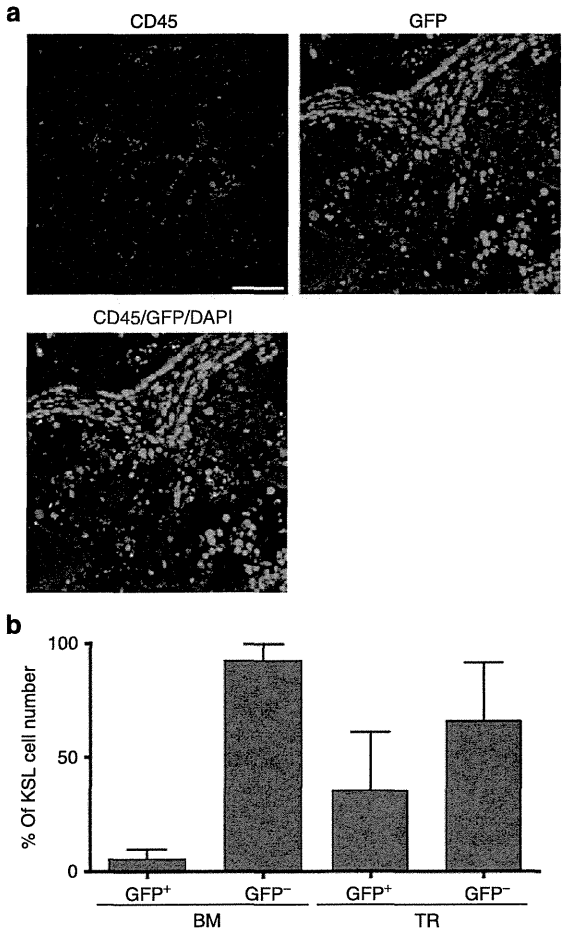

Figure 4 Hematopoietic stem cell (HSC) niche environment formation in GFP-iPSC–derived teratomas. (**a**) Immunostaining of CD45$^+$ cells in G-iPSC–derived teratomas. Bar, 75 μm. (**b**) Flow cytometric analysis of iPSC-derived GFP$^+$ and GFP$^-$ CD45$^+$ cells and KSL cells in bone marrow (BM) and teratomas (TR). KSL cells in teratomas ranging from 93 to 620 cells. DAPI, 4′,6-diamidino-2-phenylindole; GFP, green fluorescent protein; G-iPSC, *GFP* transgenic mice-induced pluripotent stem cell.

within teratomas with the aid of host-derived myeloid cells. GFP$^+$ KSL cells were also identifiable by fluorescence-activated cell sorting analysis, suggesting that HSCs were generated from iPSCs in teratomas (**Figure 4b**). Osteoblasts,[26,27] endothelial cells,[28,29] and nonmyelinating Schwann cells[30] are believed to contribute to formation of the HSC niche.[31] We immunohistochemically confirmed a large number of osteocalcin$^+$ osteoblasts as well as VE-cadherin$^+$ endothelial cells in G-iPSC–derived teratoma sections (**Supplementary Figure S5c**). Moreover, CD45$^+$ c-Kit$^+$ cells presumably containing HSCs were found localized near VE-cadherin$^+$ cells and osteocalcin$^+$ cells (**Supplementary Figure S5d,e**). In human iPSC-derived teratomas, CD45$^+$ CD34$^+$ HSCs were frequently observed near HSC niche-like cells (**Supplementary Figure S5a,b**). Collectively these data clearly indicate that HSCs and the previously reported niche components co-exist in teratomas.

DISCUSSION

HSCs are the best-studied stem cells with a number of *in vitro* as well as *in vivo* assay systems. Yet, *in vitro* generation of HSCs from ESCs or iPSCs is difficult even with genetic modification. In this study, we succeeded in inducing HSCs by injecting iPSCs into immunodeficient mice and reproducing the HSC niche subcutaneously by way of teratoma formation. Although injection of iPSCs alone could not generate iPSC-derived HSCs, co-injection of iPSCs with OP9 stromal cells along with hematopoietic cytokines dramatically enhanced the induction efficiency. We confirmed that HSCs derived from both LG- and G-iPSCs could self-renew and reconstitute multiple lineages by transplanting BM cells of teratoma-bearing mice. Prospectively isolated LG- and G-iPSC–derived CD34$^-$ KSL cells could give rise to all blood lineages on secondary transfer. These findings strongly suggested that injected iPSCs partially differentiate into HSCs in teratomas and migrate into BM of teratoma-bearing mice, the iPSC-derived HSCs being indistinguishable from bona fide HSCs with regard to phenotype and biological characteristics. This is in contrast to the HSCs generated *in vitro* from PSCs, which lack homing capacity, thus requiring additional use of an intra-BM delivery method.[32–34] Unlike *in vitro* culture systems, microenvironment present in a teratoma must have been very similar to that prevailing during normal embryonic development. During the course of the study, we performed transplantation of HSCs directly isolated from teratomas and found that these maintain a stable reconstitution ability. However, because of a significantly high level of lethality, we could not observe long-term repopulation. This is probably due to contamination of iPSC-like immature cells in HSCs fractions. These results suggest that only functional HSCs were selected in the process of BM homing. Similar findings were also reported by Amabile *et al.*,[35] but here we carefully investigated the optimal conditions for *in vivo* induction of HSCs using *Lnk*$^{-/-}$ mice. Furthermore, we demonstrated, as proof-of-principle, that gene correction in X-SCID mice-derived iPSCs could overcome immunodeficiency by generation of T lymphocytes with HSCs through teratoma formation. Finally, human iPSCs also proved capable of generating functional HSCs in xenogenic mouse models, reconstituting myeloid and lymphoid cells in recipient mice with intravenous transplantation.

Gene therapy of HSCs is currently limited due to substantial risks of leukemogenesis caused by viral-mediated insertional mutagenesis.[22,23] In contrast, clonal selection of gene-corrected iPSCs derived from patients with defined proviral insertion in the secure genome region may be more appropriate for therapeutic application because screened iPSCs can be expanded clonally *ex vivo*.[24] In addition, leukemia and other hematopoietic abnormalities have not been observed in recipient mice, suggesting that these iPSC-derived HSCs generated in teratomas are functionally and developmentally normal. Compared with those developing *in vitro*, HSCs obtained from teratomas must have gone through the near-normal differentiation processes with appropriate epigenetic changes utilizing the microenvironment offered by a teratoma.

Since this system made it possible to generate engraftable HSCs from ESCs/iPSCs, it should provide a useful tool for the study of HSC biology. In addition, our differentiation system can expect to find application in elucidation of mechanisms and development of drugs for various hematopoietic diseases by analyzing iPSC-derived HSCs or terminally differentiated blood cells. There are a number of issues that remain to be clarified before this

system could be used for generation of clinically usable human HSCs, but eventually we should be able to transplant a patient's own gene-corrected iPSC-derived HSCs isolated from BM of teratoma-bearing immunodeficient animals.

We believe that our novel technique will be an exciting research tool having therapeutic potential which will open up a new era for both custom-tailored cell therapy and disease modeling using iPSCs.

MATERIALS AND METHODS

Mice. C57BL/6 (B6) mice, KSN/Slc nude mice, and *GFP* transgenic mice were purchased from Japan SLC (Shizuoka, Japan). *Lnk*$^{-/-}$ *GFP* transgenic mice were bred and maintained in the Animal Research Facility of the Institute of Medical Science, University of Tokyo. Generation and characterization of X-SCID mice with B6 background were as described earlier. NOD/SCID mice were purchased from CLEA Japan (Tokyo, Japan) and NOD/SCID/JAK3^{null} mice from Sankyo Labo Service (Tokyo, Japan). Animal care in our laboratory was in accordance with the guidelines of University of Tokyo for animal and recombinant DNA experiments.

Cell lines and culture conditions. Mouse iPSCs were obtained by reprogramming tail tip fibroblasts of *Lnk*$^{-/-}$ *GFP* transgenic B6 mice and *GFP* transgenic B6 mice with *Oct3/4*, *Sox2*, and *Klf4*, then maintained on mouse embryonic fibroblasts with iPSCs culture medium consisting of Dulbecco's Modified Eagle Medium (GIBCO, Carlsbad, CA) supplemented with 15% Knockout Serum Replacement (GIBCO), 20 mmol/l HEPES buffer solution, 0.1 mmol/l minimum essential medium (MEM) non-essential amino acids solution, 0.1 mmol/l L-glutamine (Invitrogen, Carlsbad, CA), 100 U/ml penicillin, 100 μg/ml streptomycin (Sigma-Aldrich, St Louis, MO), 0.1 mmol/l 2-mercaptoethanol, and 1,000 U/ml ESGRO (GIBCO).

Human iPSCs were obtained by reprogramming adult normal human epidermal keratinocytes (Lonza, Basel, Switzerland) with *Oct3/4*, *Sox2*, and *Klf4*. Established iPSCs were maintained on mouse embryonic fibroblasts with culture medium consisting of Dulbecco's Modified Eagle Medium-F12 (Sigma-Aldrich) supplemented with 20% Knockout SR, 0.1 mmol/l MEM non-essential amino acids solution (Invitrogen), 0.2 mmol/l L-glutamine, 0.1 mmol/l 2-mercaptoethanol, and 5 ng/ml bFGF (PeproTech, Rocky Hill, NJ).

OP9 cells were maintained in growth medium consisting of MEM α-medium (α-MEM; Invitrogen), supplemented with 20% fetal bovine serum (HyClone, Logan, UT).

Histopathology and immunostaining. Histological findings were assessed by light microscopy of hematoxylin and eosin-stained sections of paraffin-embedded teratoma tissue.

Immunofluorescence staining of Nanog and SSEA-1 was performed using cryosections with an anti-mouse Nanog antibody (1:100; Cosmo Bio, Tokyo, Japan) and an anti-mouse SSEA-1 antibody (1:100; Abcam, Cambridge, MA), followed by incubation with anti-rabbit IgG coupled with Alexa Fluor 546 (1:300; Invitrogen) and with anti-mouse IgM-allophycocyanin (APC) (1:100; eBioscience, San Diego, CA). Nuclei were counterstained with 4',6-diamidino-2-phenylindole (DAPI; Sigma-Aldrich) according to the manufacturer's instructions. Sections were viewed and images were captured using an Olympus BX-51 fluorescence microscope and digital camera system DP-71 (OLYMPUS, Tokyo, Japan).

Teratoma tissues were embedded in Optimal Cutting Temperature (O.C.T.) compound (Sakura Finetek, Tokyo, Japan) and flash-frozen on dry ice. Then 7–8 μm sections produced using a CM3050 S cryostat (Leica Microsystems, Tokyo, Japan) were fixed with ethanol and immunostained. Each section was incubated with primary antibodies for 24 hours at 4 °C and with secondary antibodies for 30 minutes at room temperature. Primary antibodies, all anti-mouse, were directed against CD45 (1:50; BD Biosciences, San Jose, CA), osteocalcin (1:200; LifeSpan Biosciences, Seattle, WA), and VE-cadherin (1:200; Abcam). CD117 was stained with Alexa Fluor 488-conjugated anti-mouse antibody (1:10; BioLegend, San Diego, CA). Secondary antibodies were Alexa Fluor 546-conjugated goat anti-rat IgG and Alexa Fluor 647-conjugated goat anti-rabbit IgG (Invitrogen). After antibody treatment, sections were mounted employing a fluorescence-microscopy medium (Dako, Carpinteria, CA) containing DAPI (Sigma-Aldrich) for nuclear counterstaining. Sections were examined under a TCS SP2 AOBS confocal laser scanning microscope (Leica Microsystems).

Teratoma formation and differentiation of iPSCs to HSCs

Mouse iPSCs. 5×10^6 iPSCs were injected subcutaneously into KSN/Slc mice (4–5 weeks old). Differentiation of HSCs was induced under the following conditions: (i) only iPSCs were injected as a control; (ii) the hematopoietic cytokines SCF (200 ng) and TPO (200 ng) (PeproTech) were administered *via* a micro-osmotic pump (ALZET, Cupertino, CA) implanted subcutaneously for 2 weeks; (iii) 1×10^6 OP9 stromal cells were co-transplanted with iPSCs; and (iv) both cytokines and OP9 cells were administered.

Human iPSCs. 1×10^6 iPSCs and 5×10^5 OP9 stromal cells were co-injected into testes of NOD/SCID mice (5–7 weeks old). The hematopoietic cytokines human recombinant SCF (200 ng) and TPO (200 ng) (PeproTech) were administered *via* a micro-osmotic pump (ALZET) implanted subcutaneously for 2 weeks.

Flow cytometry analysis and sorting

Mouse iPSC-derived blood cells. Mouse PB and spleen cells were stained with anti-mouse antibodies, APC-conjugated anti-CD45 (BD Biosciences), APC-Cy7–conjugated anti-CD3e, Pacific Blue-conjugated anti-CD45R (eBioscience), phycoerythrin (PE)-Cy7–conjugated anti-Gr-1, and anti-Mac-1 (BioLegend). BM cells of teratoma-bearing mice were extracted by flushing out. They were stained with an antibody mixture consisting of anti-mouse biotinylated anti-Gr-1, anti-Mac-1, anti-CD45R, anti-CD4, anti-CD8, anti-IL-7R, and anti-TER119 antibodies (eBioscience) and Lin$^+$ cells were then depleted using MACS anti-biotin microbeads and a LS-MACS system (Miltenyi Biotec, Bergisch Gladbach, Germany). The cells were further stained with anti-mouse Alexa Fluor 700-conjugated anti-CD34, Pacific Blue-conjugated anti-Sca-1, and APC-conjugated anti-CD117 antibodies, as well as with APC-Cy7–conjugated streptavidin antibody for biotinylated antibodies (eBioscience). Four color analysis and sorting were performed on a FACSAria (Becton Dickinson, Franklin Lakes, NJ).

hiPSC-derived blood cells. BM cells of teratoma-bearing mice were stained with APC-conjugated anti-mouse CD45, fluorescein isothiocyanate-conjugated anti-human CD34 (BD Biosciences), and Pacific Blue-conjugated anti-human CD45 antibodies (BioLegend). PB of recipient mice was stained with APC-conjugated anti-mouse CD45, PE-conjugated anti-human CD3, APC-H7–conjugated anti-human CD19, PE-Cy7–conjugated anti-human CD33 (BD Biosciences), and Pacific Blue-conjugated anti-human CD45 antibodies (BioLegend). Analysis and sorting were performed on a FACSAria (Becton Dickinson).

Teratoma-derived blood cells. Teratomas were minced into small pieces and digested in 0.2% collagenase (Wako Pure Chemical Industries, Osaka, Japan) for 30 minutes with shaking at 37 °C. The suspension was filtered with a cell strainer (Falcon 2350) and collected by centrifugation at 280*g* for 7 minutes at 4 °C. The pellet was immersed in 1 ml water (Sigma-Aldrich) for 5–10 seconds to burst the RBCs, after which 1 ml of 2× phosphate-buffered saline (dilution from Sigma-Aldrich) containing 4% fetal bovine serum was added, and the suspension was filtered through a cell strainer. Cell staining and analysis were same as BM cells.

Single-cell colony assay. Purified iPSC-derived CD34$^-$ KSL cells were clonally deposited into 96-well plates containing 200 μl of S-clone SF-O3 medium (Sanko Junyaku, Tokyo, Japan) supplemented with 1% bovine serum albumin and mouse SCF (50 ng/ml), TPO (50 ng/ml), IL-3

(10 ng/ml), and EPO (1 U/ml; all PeproTech). The cells were incubated at 37 °C in a humidified atmosphere with 5% CO_2. Ten days after incubation began the cells were cytospun onto slide glasses and stained using Hemacolor (Merck, Darmstadt, Germany).

BM transplantation assay

LG-iPSC-derived HSCs. 1×10^7 BM cells of teratoma-bearing mice were transplanted into lethally irradiated (9.5 Gy) wild-type B6 recipient mice. Four and 12 weeks thereafter, PB cells of recipient mice were analyzed by flow cytometry. 1×10^7 BM cells of primary recipient mice were secondarily transplanted 12 weeks after primary BM transplantation.

G-iPSC-derived HSCs. 40 GFP^+ $CD34^-$ KSL cells of primary recipient mice were sorted and transplanted into secondary recipient mice with 2×10^5 B6 BM cells.

hiPSC-derived HSCs. 1×10^7 BM cells or 600 mCD45-depleted $hCD45^+$ $hCD34^+$ BM cells with 2×10^5 NOD/SCID BM cells of teratoma-bearing mice were transplanted into irradiated (2 Gy) NOD/SCID or NOD/SCID/$JAK3^{null}$ recipient mice. Eight weeks after transplantation, PB cells of recipient mice were analyzed by flow cytometry.

Statistical analysis. Mean values of two groups were compared by two-tailed unpaired *t*-testing. All statistical analyses were performed on Prism 4 software (Graphpad, San Diego, CA).

SUPPLEMENTARY MATERIAL

Figure S1. Engraftable HSCs were induced from LG-iPSCs through teratoma formation.

Figure S2. Engraftable HSCs were induced from G-iPSCs through teratoma formation.

Figure S3. Establishment of gene-corrected mγc-iPSCs from X-SCID mice.

Figure S4. Induction of engraftable HSCs from hiPSCs through teratoma formation.

Figure S5. iPSC-derived hematopoietic cells including HSCs and HSC niche components were co-exist in teratomas.

Table S1. Chimerism of iPS-derived hematopoietic cells in recipient mice 12 weeks after bone marrow transplantation.

ACKNOWLEDGMENTS

We thank Kazuo Sugamura and Naoto Ishii for the X-linked severe combined immunodeficiency mice, Yumiko Ishii and Stephanie Napier for technical assistance, and Masataka Kasai, Hideo Ema, and A.S. Knisely for critical review of the manuscript. This work was supported in part by grants from the Ministry of Education, Culture, Sport, Science and Technology, Japan. The authors declared no conflict of interest.

REFERENCES

1. Takahashi, K and Yamanaka, S (2006). Induction of pluripotent stem cells from mouse embryonic and adult fibroblast cultures by defined factors. *Cell* **126**: 663–676.
2. Okita, K, Ichisaka, T and Yamanaka, S (2007). Generation of germline-competent induced pluripotent stem cells. *Nature* **448**: 313–317.
3. Takahashi, K, Tanabe, K, Ohnuki, M, Narita, M, Ichisaka, T, Tomoda, K *et al.* (2007). Induction of pluripotent stem cells from adult human fibroblasts by defined factors. *Cell* **131**: 861–872.
4. Takayama, N, Nishimura, S, Nakamura, S, Shimizu, T, Ohnishi, R, Endo, H *et al.* (2010). Transient activation of c-MYC expression is critical for efficient platelet generation from human induced pluripotent stem cells. *J Exp Med* **207**: 2817–2830.
5. Loh, YH, Wu, Q, Chew, JL, Vega, VB, Zhang, W, Chen, X *et al.* (2006). The Oct4 and Nanog transcription network regulates pluripotency in mouse embryonic stem cells. *Nat Genet* **38**: 431–440.
6. Choi, KD, Yu, J, Smuga-Otto, K, Salvagiotto, G, Rehrauer, W, Vodyanik, M *et al.* (2009). Hematopoietic and endothelial differentiation of human induced pluripotent stem cells. *Stem Cells* **27**: 559–567.
7. Kyba, M, Perlingeiro, RC and Daley, GQ (2002). HoxB4 confers definitive lymphoid-myeloid engraftment potential on embryonic stem cell and yolk sac hematopoietic progenitors. *Cell* **109**: 29–37.
8. Pilat, S, Carotta, S, Schiedlmeier, B, Kamino, K, Mairhofer, A, Will, E *et al.* (2005). HOXB4 enforces equivalent fates of ES-cell-derived and adult hematopoietic cells. *Proc Natl Acad Sci USA* **102**: 12101–12106.
9. Wang, L, Menendez, P, Shojaei, F, Li, L, Mazurier, F, Dick, JE *et al.* (2005). Generation of hematopoietic repopulating cells from human embryonic stem cells independent of ectopic HOXB4 expression. *J Exp Med* **201**: 1603–1614.
10. Ledran, MH, Krassowska, A, Armstrong, L, Dimmick, I, Renström, J, Lang, R *et al.* (2008). Efficient hematopoietic differentiation of human embryonic stem cells on stromal cells derived from hematopoietic niches. *Cell Stem Cell* **3**: 85–98.
11. Risueño, RM, Sachlos, E, Lee, JH, Lee, JB, Hong, SH, Szabo, E *et al.* (2012). Inability of human induced pluripotent stem cell-hematopoietic derivatives to downregulate microRNAs *in vivo* reveals a block in xenograft hematopoietic regeneration. *Stem Cells* **30**: 131–139.
12. Cudennec, C and Nicolas, JF (1977). Blood formation in a clonal cell line of mouse teratocarcinoma. *J Embryol Exp Morphol* **38**: 203–210.
13. Cudennec, CA and Salaün, J (1979). Definitive red blood cell differentiation in a clonal line of mouse teratocarcinoma cultured *in vivo* in the chick embryo. *Cell Differ* **8**: 75–82.
14. Cudennec, CA and Johnson, GR (1981). Presence of multipotential hemopoietic cells in teratocarcinoma cultures. *J Embryol Exp Morphol* **61**: 51–59.
15. Li, Z, Huang, H, Boland, P, Dominguez, MG, Burfeind, P, Lai, KM *et al.* (2009). Embryonic stem cell tumor model reveals role of vascular endothelial receptor tyrosine phosphatase in regulating Tie2 pathway in tumor angiogenesis. *Proc Natl Acad Sci USA* **106**: 22399–22404.
16. Bhattacharya, D, Czechowicz, A, Ooi, AG, Rossi, DJ, Bryder, D and Weissman, IL (2009). Niche recycling through division-independent egress of hematopoietic stem cells. *J Exp Med* **206**: 2837–2850.
17. Wagers, AJ, Sherwood, RI, Christensen, JL and Weissman, IL (2002). Little evidence for developmental plasticity of adult hematopoietic stem cells. *Science* **297**: 2256–2259.
18. Seita, J, Ema, H, Ooehara, J, Yamazaki, S, Tadokoro, Y, Yamasaki, A *et al.* (2007). Lnk negatively regulates self-renewal of hematopoietic stem cells by modifying thrombopoietin-mediated signal transduction. *Proc Natl Acad Sci USA* **104**: 2349–2354.
19. Takaki, S, Morita, H, Tezuka, Y and Takatsu, K (2002). Enhanced hematopoiesis by hematopoietic progenitor cells lacking intracellular adaptor protein, Lnk. *J Exp Med* **195**: 151–160.
20. Ema, H, Sudo, K, Seita, J, Matsubara, A, Morita, Y, Osawa, M *et al.* (2005). Quantification of self-renewal capacity in single hematopoietic stem cells from normal and Lnk-deficient mice. *Dev Cell* **8**: 907–914.
21. Buckley, RH, Schiff, RI, Schiff, SE, Markert, ML, Williams, LW, Harville, TO *et al.* (1997). Human severe combined immunodeficiency: genetic, phenotypic, and functional diversity in one hundred eight infants. *J Pediatr* **130**: 378–387.
22. Hacein-Bey-Abina, S, Garrigue, A, Wang, GP, Soulier, J, Lim, A, Morillon, E *et al.* (2008). Insertional oncogenesis in 4 patients after retrovirus-mediated gene therapy of SCID-X1. *J Clin Invest* **118**: 3132–3142.
23. Howe, SJ, Mansour, MR, Schwarzwaelder, K, Bartholomae, C, Hubank, M, Kempski, H *et al.* (2008). Insertional mutagenesis combined with acquired somatic mutations causes leukemogenesis following gene therapy of SCID-X1 patients. *J Clin Invest* **118**: 3143–3150.
24. Hanna, J, Wernig, M, Markoulaki, S, Sun, CW, Meissner, A, Cassady, JP *et al.* (2007). Treatment of sickle cell anemia mouse model with iPS cells generated from autologous skin. *Science* **318**: 1920–1923.
25. Chang, KH, Nelson, AM, Cao, H, Wang, L, Nakamoto, B, Ware, CB *et al.* (2006). Definitive-like erythroid cells derived from human embryonic stem cells coexpress high levels of embryonic and fetal globins with little or no adult globin. *Blood* **108**: 1515–1523.
26. Calvi, LM, Adams, GB, Weibrecht, KW, Weber, JM, Olson, DP, Knight, MC *et al.* (2003). Osteoblastic cells regulate the haematopoietic stem cell niche. *Nature* **425**: 841–846.
27. Zhang, J, Niu, C, Ye, L, Huang, H, He, X, Tong, WG *et al.* (2003). Identification of the haematopoietic stem cell niche and control of the niche size. *Nature* **425**: 836–841.
28. Li, W, Johnson, SA, Shelley, WC and Yoder, MC (2004). Hematopoietic stem cell repopulating ability can be maintained *in vitro* by some primary endothelial cells. *Exp Hematol* **32**: 1226–1237.
29. Avecilla, ST, Hattori, K, Heissig, B, Tejada, R, Liao, F, Shido, K *et al.* (2004). Chemokine-mediated interaction of hematopoietic progenitors with the bone marrow vascular niche is required for thrombopoiesis. *Nat Med* **10**: 64–71.
30. Yamazaki, S, Ema, H, Karlsson, G, Yamaguchi, T, Miyoshi, H, Shioda, S *et al.* (2011). Nonmyelinating Schwann cells maintain hematopoietic stem cell hibernation in the bone marrow niche. *Cell* **147**: 1146–1158.
31. Kiel, MJ, Yilmaz, OH, Iwashita, T, Yilmaz, OH, Terhorst, C and Morrison, SJ (2005). SLAM family receptors distinguish hematopoietic stem and progenitor cells and reveal endothelial niches for stem cells. *Cell* **121**: 1109–1121.
32. Tian, X, Woll, PS, Morris, JK, Linehan, JL and Kaufman, DS (2006). Hematopoietic engraftment of human embryonic stem cell-derived cells is regulated by recipient innate immunity. *Stem Cells* **24**: 1370–1380.
33. Burt, RK, Verda, L, Kim, DA, Oyama, Y, Luo, K and Link, C (2004). Embryonic stem cells as an alternate marrow donor source: engraftment without graft-versus-host disease. *J Exp Med* **199**: 895–904.
34. Sasaki, K, Nagao, Y, Kitano, Y, Hasegawa, H, Shibata, H, Takatoku, M *et al.* (2005). Hematopoietic microchimerism in sheep after in utero transplantation of cultured cynomolgus embryonic stem cells. *Transplantation* **79**: 32–37.
35. Amabile, G, Welner, RS, Nombela-Arrieta, C, D'Alise, AM, Di Ruscio, A, Ebralidze, AK *et al.* (2013). *In vivo* generation of transplantable human hematopoietic cells from induced pluripotent stem cells. *Blood* **121**: 1255–1264.

Journal of Biotechnology 168 (2013) 659–665

Contents lists available at ScienceDirect

Journal of Biotechnology

journal homepage: www.elsevier.com/locate/jbiotec

Top-down motif engineering of a cytokine receptor for directing ex vivo expansion of hematopoietic stem cells

Koichiro Saka[a], Masahiro Kawahara[a,*], Jinying Teng[a], Makoto Otsu[b], Hiromitsu Nakauchi[b], Teruyuki Nagamune[a]

[a] Department of Chemistry and Biotechnology, School of Engineering, The University of Tokyo, 7-3-1 Hongo, Bunkyo-ku, Tokyo 113-8656, Japan
[b] Division of Stem Cell Therapy, Center for Stem Cell Biology and Regenerative Medicine, Institute of Medical Science, The University of Tokyo, 4-6-1, Shirokanedai, Minato-ku, Tokyo 108-8639, Japan

ARTICLE INFO

Article history:
Received 11 September 2013
Accepted 12 September 2013
Available online 23 September 2013

Keywords:
Cytokine receptor
Signal transduction
Tyrosine motif
Hematopoietic stem cell
Chimeric protein

ABSTRACT

The technique to expand hematopoietic stem cells (HSCs) ex vivo is eagerly anticipated to secure an enough amount of HSCs for clinical applications. Previously we developed a scFv-thrombopoietin receptor (c-Mpl) chimera, named S-Mpl, which can transduce a proliferation signal in HSCs in response to a cognate antigen. However, a remaining concern of the S-Mpl chimera may be the magnitude of the cellular expansion level driven by this molecule, which was significantly less than that mediated by endogenous wild-type c-Mpl. In this study, we engineered a tyrosine motif located in the intracellular domain of S-Mpl based on a top-down approach in order to change the signaling properties of the chimera. The truncated mutant (trunc.) and an amino-acid substitution mutant (Q to L) of S-Mpl were constructed to investigate the ability of these mutants to expand HSCs. The result showed that the truncated and Q to L mutants gave higher and considerably lower number of the cells than unmodified S-Mpl, respectively. The proliferation level through the truncated mutant was even higher than that of non-transduced HSCs with the stimulation of a native cytokine, thrombopoietin. Moreover, we analyzed the signaling properties of the S-Mpl mutants in detail using a pro-B cell line Ba/F3. The data indicated that the STAT3 and STAT5 activation levels through the truncated mutant increased, whereas activation of the Q to L mutant was inhibited by a negative regulator of intracellular signaling, SHP-1. This is the first demonstration that a non-natural artificial mutant of a cytokine receptor is effective for ex vivo expansion of hematopoietic cells compared with a native cytokine receptor.

1. Introduction

Since blood plays essential roles in maintaining homeostasis of our body, various blood disorders including myeloma, leukemia and anemia are life-threatening. Today, hematopoietic stem cell (HSC) transplantation is an effective treatment for these diseases. However, HSCs are rare population of blood cells, representing less than 0.01% of the bone marrow cells. Therefore, the technique to expand HSCs ex vivo is eagerly anticipated to secure an enough amount of HSCs for clinical applications.

The HSC expansion has been regulated by intrinsic and extrinsic regulators, such as cytokines and small molecules (Walasek et al., 2012). Cytokines, for example, thrombopoietin (TPO) (Ohmizono et al., 1997; Piacibello et al., 1998) and stem cell factor (SCF) (Abboud et al., 1994), together with the corresponding receptors, c-Mpl and c-Kit, respectively, are important for the maintenance of HSCs. Signal transduction from these receptors are initiated by binding of the cognate ligand, which triggers receptor oligomerization. Consequently, the intracellular kinase domain of receptors or Janus kinase (JAK), a tyrosine kinase which constitutively associates with the receptor, is activated. Accordingly, the activated kinase phosphorylates tyrosine residues located in the intracellular domain of the receptor. Signaling molecules bind to the phosphorylated tyrosine residues, and are phosphorylated by the kinase. Phosphorylated signaling molecules dissociate from the receptor, resulting in signal transduction to intracellular second messengers (Ihle, 1995; Kaushansky, 2005). The amino acid sequence surrounding the tyrosine residue determines whether a signaling molecule can bind to the tyrosine residue (Songyang et al., 1993).

Therefore, activation of these intracellular signaling molecules is crucial for the control of cellular fates through c-Mpl and c-Kit signalings. In fact, the PTEN/PI3K/Akt signaling (Datta et al., 1997; Rossi and Weissman, 2006; Salmena et al., 2008), which is activated through both TPO and SCF signalings, are known as the key regulators for ex vivo expansion and maintenance of HSCs. However, the natural cytokine-mediated expansion methods generate only

* Corresponding author. Tel.: +81 3 5841 7290; fax: +81 3 5841 8657.
E-mail address: kawahara@bio.t.u-tokyo.ac.jp (M. Kawahara).

0168-1656/$ – see front matter © 2013 Elsevier B.V. All rights reserved.
http://dx.doi.org/10.1016/j.jbiotec.2013.09.012

moderate increases in progenitor cell numbers with at best modest improvements in clinically relevant outcomes (Dahlberg et al., 2011). The robust ex vivo expansion techniques that are useful for clinical applications have yet to be accomplished.

To overcome these problems, we previously developed scFv-receptor chimeras that can transduce a signal in response to a cognate inexpensive antigen (Kaneko et al., 2012; Kawahara et al., 2011). An anti-fluorescein single-chain Fv (scFv) fused to the extracellular D2 domain of erythropoietin receptor (EpoR) was joined to the transmembrane and whole cytoplasmic domains of c-Mpl or c-Kit, resulting in the S-Mpl or S-Kit chimera, respectively. When the chimeras were expressed in interleukin (IL)-3-dependent pro-B cell line Ba/F3, genetically modified cells were selectively expanded in the presence of fluorescein-conjugated BSA (BSA-FL) as a specific antigen. Furthermore, highly purified mouse HSCs transduced with the retrovirus carrying the S-Mpl chimera gene proliferated in vitro in response to BSA-FL, and the cells retained in vivo long-term repopulating abilities (Kawahara et al., 2011). However, a remaining concern of the S-Mpl chimera may be the magnitude of the cellular expansion level driven by this molecule, which was significantly less than that mediated by endogenous wild-type c-Mpl.

In this study, to enhance the expansion levels of hematopoietic cells by S-Mpl, we engineered the intracellular domain in S-Mpl and changed the signaling properties of the chimera. Focusing on the tyrosine motif (YWQQ) located at the C-terminus of S-Mpl, we constructed the truncated mutant (trunc.) and the amino-acid substitution mutant (Q to L) of S-Mpl. We compared the ability of HSC proliferation among the original and the mutants of S-Mpl. Moreover, Ba/F3 cells were transduced with the retroviral vector carrying each chimeric receptor to examine the signaling properties of the receptors in detail by western blot.

2. Materials and methods

2.1. Plasmid construction

pBS-EMpl-IG, which encodes the extracellular D2 domain of erythropoietin receptor (EpoR), the cytoplasmic/transmembrane domains of c-Mpl and an IRES-EGFP cassette, was as described (Kawahara et al., 2011). To engineer the intracellular domain of c-Mpl, pBS-EMpl-IG was mutated by PCR using two primer sets (trunc sense: 5′-CCTACCACTAAGCTAGTGGCAGCAGCCTTG-3′, trunc antisense: 5′-CAAGGCTGCTGCCACTAGCTTAGTGGTAGG-3′ and Q to L sense: 5′-GCTATTGGCAGCTGCCTTGAGGATCCGCC-3′, Q to L antisense: 5′-GGCGGATCCTCAAGGCAGCTGCCAATAGC-3′), resulting in pBS-EMpl(trunc.)-IG and pBS-EMpl(Q to L)-IG, respectively. To utilize the GCDNsam retroviral expression system and to append a HA tag at the N-terminus of the chimeric receptors, pBS-EMpl-IG, pBS-EMpl(trunc.)-IG and pBS-EMpl(Q to L)-IG were digested by *Bsp*EI and *Bam*HI, and the fragments were inserted into *Bsp*EI- and *Bam*HI-digested pGCDNsam-HA-SD2g-I/E (manuscript in preparation) to obtain pGCDNsam-HA-S-Mpl(WT)-I/E, pGCDNsam-HA-S-Mpl(trunc.)-I/E and pGCDNsam-HA-S-Mpl(Q to L)- I/E, respectively.

2.2. Animals and cell lines

C57BL/6-Ly5.1 mice were purchased from Japan SLC (Shizuoka, Japan). The Animal Experiment Committee of the Institute of Medical Science, The University of Tokyo, approved all animal care and use in this study.

A murine IL-3-dependent pro-B cell line, Ba/F3 (RCB0805, RIKEN Cell Bank, Tsukuba, Japan), was cultured in RPMI 1640 medium (Nissui Pharmaceutical, Tokyo, Japan) supplemented with 10% fetal bovine serum (FBS) (Biowest, Paris, France) and 1 ng/ml murine IL-3 (R&D systems, Cambridge, MA). Three retroviral packaging cell line were used; Plat-E (Morita et al., 2000) was cultured in Dulbecco's modified Eagle's medium (DMEM) (Nissui Pharmaceutical) supplemented with 10% FBS, 1 μg/ml puromycin (Sigma, St Louis, MO) and 10 μg/ml blasticidin (Kaken Pharmaceutical, Tokyo, Japan); 293GP (Burns et al., 1993) was cultured in DMEM supplemented with 10% FBS, and 293GPG (Ory et al., 1996) was cultured in DMEM supplemented with 10% FBS, 2 μg/ml puromycin, 300 μg/ml G418 (Calbiochem, Darmstadt, Germany) and 1 μg/ml tetracycline (Sigma).

2.3. Purification of murine CD34⁻KSL HSCs

$CD34^{-/low}c\text{-}Kit^{+}Sca\text{-}1^{+}Lin^{-}$ ($CD34^{-}KSL$) HSCs were purified from bone marrow of C57BL/6-Ly5.1 mice, as previously described (Osawa et al., 1996). Briefly, bone marrow cells were stained with a lineage antibody mixture consisting of anti-Gr-1, Mac-1, B220, CD4, CD8, IL-7R and Ter-119 monoclonal antibodies (BD Biosciences, Franklin Lakes, NJ), and magnetic beads-conjugated anti-rat IgG secondary antibody (Miltenyi, Auburn, CA), followed by depletion of lineage-positive cells using magnetic cell sorting. The cells were subsequently stained with phycoerythrin (PE)-conjugated anti–Sca-1, allophycocyanin (APC)-conjugated anti–c-Kit, fluorescein isothiocyanate (FITC)-conjugated anti-CD34 and biotin-conjugated lineage antibodies (all from BD Biosciences) and APC-Cy7-conjugated streptavidin (Molecular Probes, Eugene, OR). $CD34^{-}KSL$ HSCs were sorted at 400 cells/well into a 96-well plate containing α-MEM with 1% FBS, 100 ng/ml TPO and 100 ng/ml stem cell factor (SCF) (Peprotech, Rocky Hill, NJ) using a MoFlo Cell Sorter (Beckman Coulter, Fullerton, CA).

2.4. Vector transduction

Plat-E cells were transfected with the constructed plasmids using Lipofectamine LTX (Invitrogen, Groningen, The Netherlands) according to the manufacturer's protocol. The culture supernatant on day 2 was used for retroviral transduction of Ba/F3 cells in the presence of 1 ng/ml IL-3 in a 24-well plate, using RetroNectin (Takara Bio, Otsu, Shiga, Japan) according to the manufacturer's instructions.

For the transduction of mouse $CD34^{-}KSL$ HSCs, a stable virus producer cell line based on 293GPG cells was established. A retroviral packaging cell line 293GP was co-transfected with pGCDNsam variants encoding the chimeric receptors and pcDNA3.1-VSV-G encoding a VSV-G envelope gene by lipofection for a transient production of VSV-G pseudotyped retroviruses. The culture medium of the transfected 293GP was collected and subsequently used for transduction of 293GPG, which had been engineered to express the VSV-G protein under control of a tetracycline-inducible system (Ory et al., 1996). 293GPG cells transduced with GCDNsam-HA-S-Mpl-I/E, GCDNsam-HA-S-Mpl(trunc.)-I/E, GCDNsam-HA-S-Mpl(Q to L)-I/E or GCDNsam-I/E stably produced retroviruses encoding the respective genes. The culture supernatant of the transduced 293GPG was collected and centrifuged at 6000 × *g* for 16 h at 4 °C, followed by resuspension of the viral pellet in α-MEM to obtain a 100-fold concentrated virus. $CD34^{-}KSL$ HSCs cultured overnight after sorting were transduced with the virus at multiplicity of infection (MOI) of 500 in the presence of SCF and TPO (50 ng/ml each) in a 96-well plate, using RetroNectin.

2.5. In vitro growth assay of HSCs

The medium of the transduced $CD34^{-}KSL$ HSCs was exchanged into S-clone SF-03 (Sanko Junyaku Inc., Tokyo, Japan) containing 50 ng/ml SCF and 50 ng/ml TPO on the day after transduction, and the cells were cultured for 2 days. The cells were washed with

PBS containing 2% FBS. EGFP-positive transduced CD34$^-$KSL HSCs were sorted at 60 cells/well into 96-well plates with 50 ng/ml SCF, 50 ng/ml TPO plus 50 ng/ml SCF, or 50 ng/ml SCF plus 5 μg/ml BSA-FL in the S-clone SF-03 using a MoFlo Cell Sorter. After cell culture for 7 days, the cells were mixed with Flow-count (Beckman Coulter) to analyze the cell number using a FACSCalibur flow cytometer (BD Biosciences).

2.6. Sorting of the transduced cells

Sorting of EGFP-positive Ba/F3 transductants was performed with a FACSCalibur flow cytometer with excitation at 488 nm and fluorescence detection at 530 ± 15 nm in a single cell mode.

2.7. Measuring surface expression levels of HA-tagged chimeric receptors

Surface expression levels of HA-tagged chimeric receptors were measured with flow cytometry. Briefly, the EGFP-positive cells cultured in IL-3 were incubated for 30 min with 1:100 diluted mouse monoclonal anti-HA antibody (Covance, Princeton, NJ) at 4 °C, washed twice with PBS, and incubated with 1:100 diluted R-phycoerythrin (PE)-conjugated donkey F(ab′)$_2$ anti-mouse IgG secondary antibody (Jackson ImmunoResearch, West Grove, PA) at 4 °C. Cells were washed twice with PBS and analyzed with a FACSCalibur flow cytometer with excitation at 488 nm and fluorescence detection at 585 ± 21 nm.

2.8. Starvation and stimulation of cells

The EGFP-positive cells cultured in 1 ng/ml IL-3 were washed three times and cultured in depletion medium without IL-3 at 37 °C for 12 h, and then stimulated with 1 ng/ml IL-3 or 1 μg/ml BSA-FL (Sigma) at 37 °C for specified time. Ice-cold 2 mM Na_3VO_4 in PBS was added to the cells to stop the reaction and inhibit dephosphorylation. The cells were collected at 400 × g, followed by preparation of lysates and western blotting.

2.9. Western blotting

EGFP-positive cells were used for western blotting. The cells (1×10^6) were washed with PBS, lysed with 100 μl of lysis buffer (20 mM HEPES (pH 7.5), 150 mM NaCl, 10% glycerol, 1% Triton X-100, 1.5 mM $MgCl_2$, 1 mM EGTA, 10 μg/ml aprotinin, 10 μg/ml leupeptin, 1 mM Na_3VO_4) and incubated on ice for 10 min. After centrifugation at 16,100 × g at 4 °C for 10 min, the supernatant was mixed with Laemmli's sample buffer and boiled. The lysate was resolved by SDS–PAGE and transferred to a nitrocellulose membrane (GE Healthcare, Buckinghamshire, UK). After the membrane was blocked either with 5% Skim milk (Wako Pure Chemical Industries, Osaka, Japan) for the detection of JAK2, STAT1, STAT3, STAT5, PI3K, Shc, SHP-2, SHP-1, HA and β-tubulin or with Blocking One-P (Nacalai Tesque, Kyoto, Japan) for the detection of phosphorylated JAK2, STAT1, STAT3, STAT5, PI3K, Shc and SHP-2. The blot was probed with rabbit primary antibodies, followed by HRP-conjugated anti-rabbit IgG (Biosource, Camarillo, CA). The rabbit primary antibodies used are: anti-phospho-JAK2 (Tyr1007/1008) (Cell Signaling Technology, Danvers, MA), anti-JAK2 (Upstate Biotechnology, Lake Placid, NY), anti-phospho-STAT1 (Tyr701) (Cell Signaling Technology), anti-STAT1 (Cell Signaling Technology), anti-phospho-STAT3 (Tyr705) (Cell Signaling Technology), anti-STAT3 (Santa Cruz Biotechnology, Santa Cruz, CA), anti-phospho-STAT5 (Tyr694) (Cell Signaling Technology), anti-STAT5 (Santa Cruz Biotechnology), anti-phospho-PI3K (Tyr508) (Santa Cruz Biotechnology), rabbit anti-PI3K (Upstate Biotechnology), anti-phospho-Shc (Tyr239/240) (Santa Cruz Biotechnology), anti-Shc (Santa Cruz Biotechnology), ant-phospho-SHP-2 (Tyr542) (Cell Signaling Technology), anti-SHP-2 (Cell Signaling Technology), anti-SHP-1 (Santa Cruz Biotechnology), anti-HA (BETHYL, Montgomery, TX) and anti-β-tubulin (Santa Cruz Biotechnology).

Detection was performed using Chemi-Lumi One (Nacalai Tesque) or Luminata Western HRP Substrates (Millipore, Billerica, MA).

2.10. Pull-down assay

The cells (1×10^7) were washed with PBS, lysed with 1 ml of lysis buffer (20 mM HEPES (pH 7.5), 150 mM NaCl, 10% glycerol, 1% Triton X-100, 1.5 mM $MgCl_2$, 1 mM EGTA, 10 μg/ml aprotinin, 10 μg/ml leupeptin) and incubated on ice for 10 min. After centrifugation at 16,100 × g at 4 °C for 10 min, the supernatant was mixed with Protein L Plus Agarose (Thermo Fisher Scientific, Waltham, MA) and rotated for 24 h at 4 °C. The agarose beads were washed twice with wash buffer 1 (50 mM Hepes (pH 7.5), 500 mM NaCl, 0.1% SDS, 0.2% Triton X-100, 5 mM EGTA) and twice with wash buffer 2 (50 mM Hepes (pH 7.5), 150 mM NaCl, 0.1% SDS, 0.1% Triton X-100, 5 mM EGTA) and boiled with Laemmli's sample buffer, followed by western blotting as described above.

3. Results

3.1. Construction of S-Mpl mutants

To improve the efficiency of ex vivo expansion of hematopoietic cells induced by S-Mpl, we focused on the Y^{631}WQQ motif located at the C-terminus of c-Mpl. Kato et al. suggested that activation of STAT5 in HSCs led to a drastic expansion of multipotential progenitors and promoted HSC self-renewal ex vivo (Kato et al., 2005). In contrast, STAT3 was demonstrated to be dispensable for the HSC maintenance in vivo, although the role of STAT3 signaling in HSCs is particularly complex and has yet to be generalized (Chung et al., 2006). Therefore, we aimed to change the properties of STAT3 and STAT5 activation by engineering the YWQQ motif of S-Mpl to expand HSCs (Fig. 1). Because the YWQQ motif of S-Mpl contains the putative STAT3 binding consensus motif (YXXQ, X: any amino acid), we constructed the mutated S-Mpl in which the motif was truncated, named "trunc.". Moreover, because YXXL consensus motif has the property of the STAT5 recruitment, we constructed the mutated S-Mpl in which the glutamine residue of the motif was changed to a leucine residue, named "Q to L" (Klingmuller et al., 1996).

3.2. Ex vivo expansion of hematopoietic cells by signaling through S-Mpl mutants

First, we compared the levels of HSC expansion between these S-Mpl mutants. Mouse HSCs were purified by flow cytometric sorting of CD34$^{-/low}$c-Kit$^+$Sca-1$^+$Lin$^-$ (CD34$^-$KSL) cells derived from the bone marrow of C57BL/6-Ly5.1 mice. To obtain high-titer retroviruses capable of transducing CD34$^-$KSL cells with high efficiency, VSV-G pseudotyped retroviruses were prepared. The retroviral packaging cell line 293GPG was transduced with GCDNsam-S-Mpl(WT, trunc. or Q to L)-I/E, resulting in stable virus-producing cell lines. The culture supernatant was 100-fold concentrated by centrifugation and used for transduction of CD34$^-$KSL cells. CD34$^-$KSL cells were also transduced with a mock vector encoding an IRES-EGFP cassette alone as a negative control.

Three days after transduction, EGFP-positive cells were sorted and cultured in the medium with SCF alone, SCF + BSA-FL or SCF + TPO. After a 7-day culture, viable cell numbers were measured using flow cytometry (Fig. 2A). The result showed that all the transductants proliferated through SCF + TPO stimulation. The viable cell

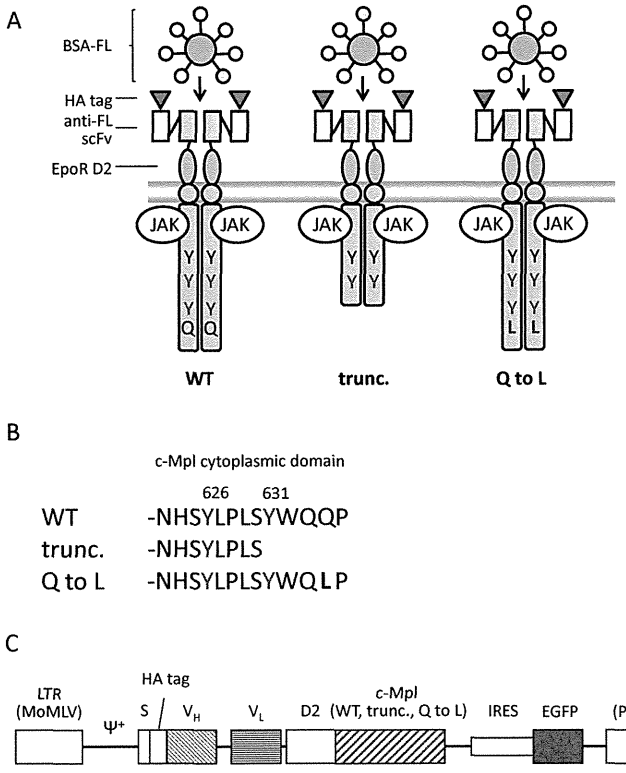

Fig. 1. The constructs of the S-Mpl mutants. (A) A schematic illustration of chimeric receptors. In the WT chimeric receptor, a HA tagged anti-fluorescein (FL) single-chain Fv (scFv) was tethered to the extracellular D2 domain of the erythropoietin receptor (EpoR D2), and the transmembrane/cytoplasmic domains of c-Mpl. In WT, three cytoplasmic tyrosine residues downstream of JAK binding region (Y^{591}, Y^{626} and Y^{631}) and Q^{634} are shown. The cytoplasmic domain of c-Mpl was engineered to make two S-Mpl mutants, "trunc." and "Q to L". (B) The C-terminal sequences of cytoplasmic domain in the mutants of S-Mpl. The amino-acid numbering is based on that for the native receptor, c-Mpl. (C) The construction of the retroviral vectors for expression of chimeric receptors. The GCDNsam retroviral vector had a 5′ Moloney murine leukemia virus (MoMLV) long terminal repeat (LTR), 3′ PCC4 cell-passaged myeloproliferative sarcoma virus (PCMV) LTR and a packaging signal (Ψ^+). An immunoglobulin κ chain secretion signal sequence (S) was placed upstream of the chimeric receptor gene for cell surface expression.

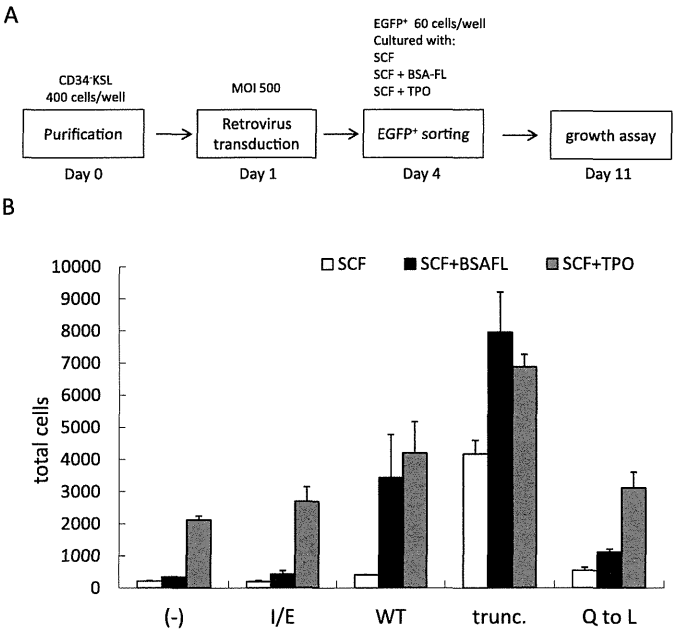

Fig. 2. Growth assay of HSCs. (A) Scheme of the HSC assay performed in vitro. CD34-KSL HSCs of B6-Ly5.1 origin were sorted into a 96-well plate at 400 cells/well on day 0 and prestimulated with SCF + TPO, followed by retroviral transduction on day 1. Three days later (day 4), the EGFP-positive cells were sorted into culture wells to test their proliferative responses in the presence of varying combinations of cytokines and BSA-FL as indicated. On day 11, the cell number was counted to compare the level of cellular expansion induced by each ligand combination. (B) Growth assay of HSCs. The numbers of cells transduced without (−) or with either GCDNsam-I/E control vector (I/E) or GCDNsam-S-Mpl(WT, trunc., Q to L)-I/E on day 11 were counted to test their proliferative responses in the indicated conditions using a FACSCalibur flow cytometer. Estimated cell numbers are shown as mean + SE of quadruplicate cultures.

numbers of (−) and I/E in the medium with SCF alone were low, and equivalent to those in the medium with SCF + BSA-FL (Fig. 2B). S-Mpl-mutant-transduced $CD34^-KSL$ cells were all expanded by SCF + BSA-FL stimulation. Of note, the truncated mutant gave significantly higher number of the cells than WT. In contrast, the Q to L mutant gave significantly lower number of the cells than WT and the truncated mutant. These results indicate that the truncated mutant can induce the proliferation of $CD34^-KSL$ cells more efficiently than WT.

3.3. Signaling properties of S-Mpl mutants

To characterize the signaling properties of the S-Mpl mutants in more detail, an IL-3-dependent murine pro-B cell line, Ba/F3, was employed because this cell line has been frequently used for functional analyses of cytokine receptors (Gow et al., 2012; Kazi and Ronnstrand, 2012). Ba/F3 cells were transduced with a retroviral vector carrying each chimeric receptor and an IRES-EGFP cassette, thus enabling identification of genetically modified cells.

First, the transductants were sorted and subjected to a flow cytometric analysis to measure EGFP-positive cell ratios. We achieved EGFP-positive cell ratios of greater than 98% for all Ba/F3 transductants (Fig. 3A). Next, the cells were stained with mouse anti-HA antibody and PE-conjugated anti-mouse IgG, and analyzed by flow cytometry to examine the surface expression levels of the HA-tagged chimeric receptors (Fig. 3B). The result showed that all Ba/F3 transductants expressed the corresponding chimeric receptors on the cell surface. When compared in median fluorescence intensity, the truncated and Q to L mutant showed 1.4 and 0.54 times as much surface expression level as WT, respectively. We also confirmed that full-length receptors were expressed in the transductants by western blot analysis using the cell lysate (Fig. 4; blot with anti-HA).

To characterize signaling property of the S-Mpl mutants, we focused on investigating the phosphorylation levels of JAK2, STAT1, STAT3, STAT5, PI3K, Shc and SHP-2. JAK2 is the kinase responsible for the phosphorylation of tyrosine motifs in the intracellular domain of type I cytokine receptors, and the other proteins are recruited to the phospho-tyrosine motifs. Phosphorylated STATs are homo- or heterodimerized, transported to the nucleus and function as transcription factors (Ivashkiv and Hu, 2004). PI3K activation induces Akt signaling (Weichhart and Saemann, 2008). Shc and SHP-2 activate the Ras-MAPK pathway (Geest and Coffer, 2009).

The Ba/F3 transductants were stimulated by BSA-FL for 15 min, and the phosphorylated intracellular signaling molecules were detected by western blot (Fig. 4). The results showed that WT and the truncated mutant activated all the signaling molecules in a BSA-FL-dependent manner. Intriguingly, the Q to L mutant showed virtually no activation of the signaling molecules including JAK2.

To find out the reason why the truncated mutant-derived signaling can enhance HSC proliferation, we compared the activation levels of STAT3 and STAT5, of which activation levels were slightly different between WT and the truncated mutant, in the time range from 15 min to 24 h (Fig. 5). The activation levels of both STAT3 and STAT5 increased at 15 min, subsequently decreased at 2 h and recovered at 6 h and 24 h. Of note, the truncated mutant

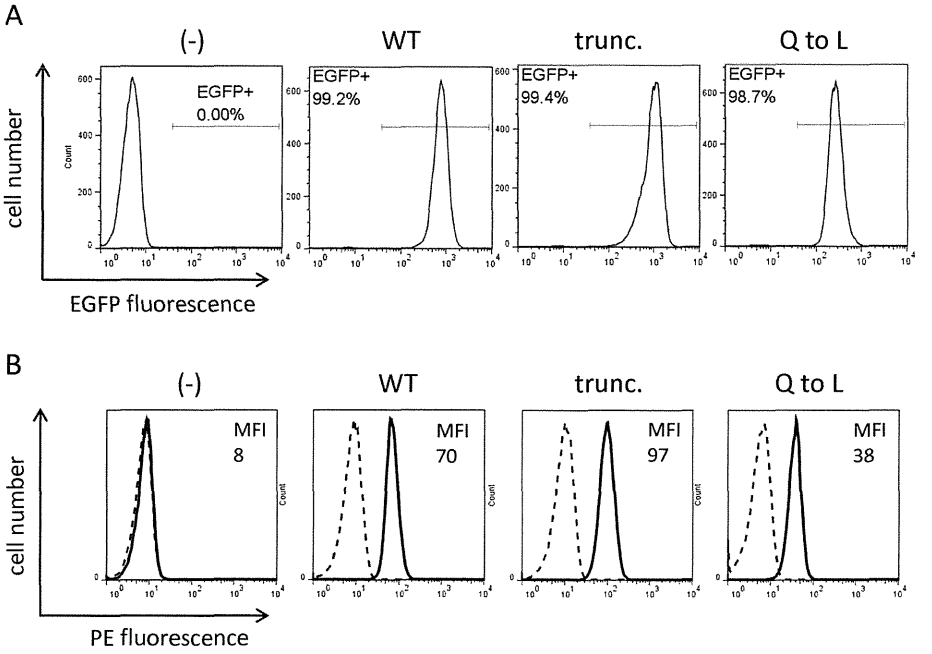

Fig. 3. Flow cytometric analyses of Ba/F3 transductants. (A) EGFP-positive cell ratio of the sorted transductants. Cell number was plotted against log green-fluorescence intensity. EGFP negative and positive regions were determined by taking parental Ba/F3 cells as a negative control. The EGFP-positive ratios are indicated. (B) Surface expression of chimeric receptors. Cell number was plotted against log PE-fluorescence intensity. The EGFP-positive cells were stained with mouse anti-HA tag antibody followed by PE-labeled secondary antibody (solid line). Median fluorescence intensity (MFI) values were shown in the histograms. Cells which were not stained with primary antibody were used as a negative control (dotted line).

gave higher signal intensity than WT in all the time points tested. Thus, the increased intracellular signaling of the truncated mutant on the cell surface induced the enhanced ex vivo expansion of hematopoietic cells.

To analyze the inhibitory effect of the Q to L mutant for HSC proliferation, we speculated the involvement of negative regulator proteins. The consensus sequence I/V/LXYXXL/V is known as an immunoreceptor tyrosine-based inhibition motif that recruits SHIP and SHP phosphatases (Daeron et al., 2008). Since the Q to L mutant contains this consensus sequence, we examined the binding of SHP-1 to the S-Mpl mutants by a pull-down assay, in which the S-Mpl mutants were pulled down with protein L-conjugated agarose beads (Fig. 6). The result showed that all the S-Mpl mutants bound to SHP-1 even without BSA-FL. Of note, the Q to L mutant bound to significantly higher amount of SHP-1 than WT and the truncated mutant, when the levels of SHP-1 binding was normalized by the

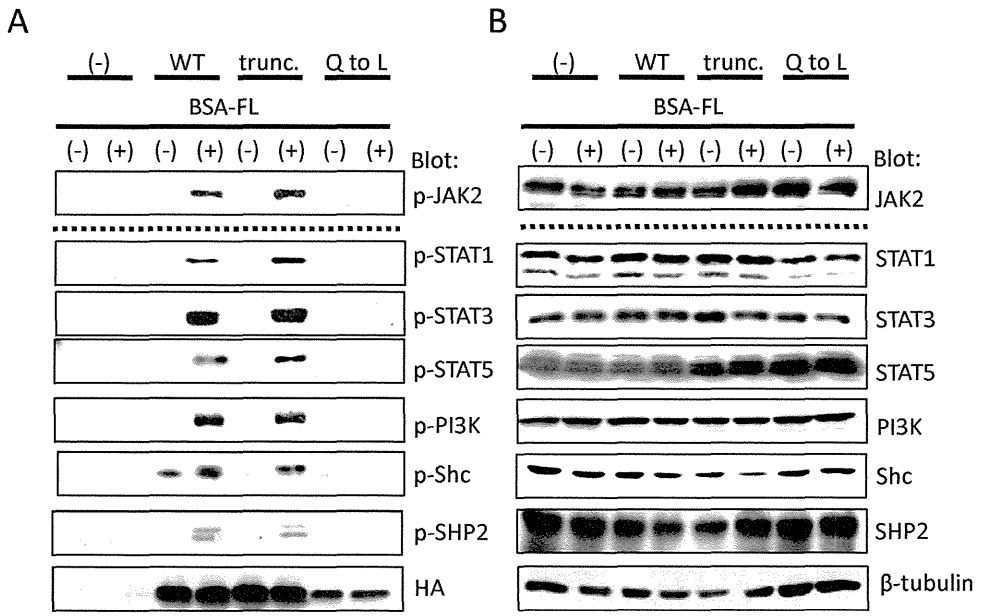

Fig. 4. BSA-FL-dependent activation of signaling molecules in the Ba/F3 transductants expressing each chimeric receptor. (A) Detection of phosphorylated signal transducers. Ba/F3 and the transductants were stimulated for 15 min with or without 1 μg/ml BSA-FL. Western blot analysis was performed with anti-phospho JAK2, STAT1, STAT3, STAT5, PI3K, Shc or SHP-2 to detect the phosphorylated form of each molecule, and with anti-HA antibody to detect the expression levels of the chimeric receptors. (B) Expression levels of signal transducers. Western blot analysis was performed with anti-JAK2, STAT1, STAT3, STAT5, PI3K, Shc, SHP-2 or β-tubulin to detect total cellular protein levels.

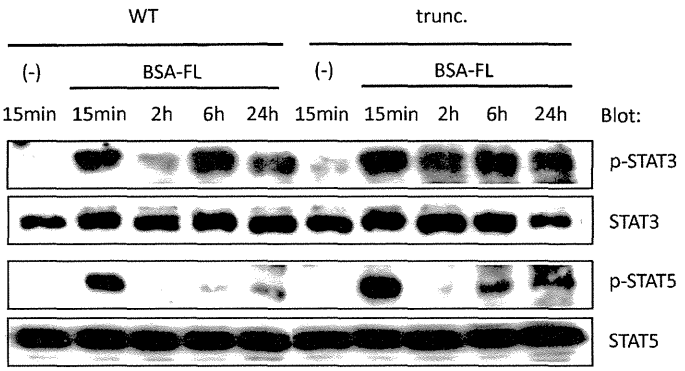

Fig. 5. Time-dependent activation levels of STAT3 and STAT5 through the chimeric receptors. Cells were stimulated for 15 min, 2 h, 6 h or 24 h with or without 1 μg/ml BSA-FL. Western blot analysis was performed to detect the phosphorylated levels and total cellular protein levels of each molecule.

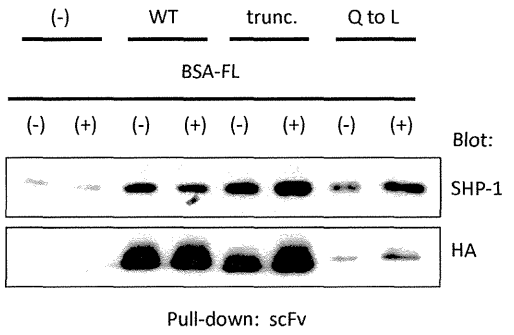

Fig. 6. Binding of negative regulator, SHP-1, to the chimeric receptors. Cells were stimulated for 15 min with or without 1 μg/ml BSA-FL. The S-Mpl chimeras of the cell lysates were pulled down by protein L-conjugated agarose beads. Western blot analysis was performed with anti-SHP-1 antibody to detect the levels of SHP-1 bound to the receptors, and with anti-HA antibody to detect the levels of each chimeric receptor pulled down by the agarose beads.

expression level of each chimeric receptor. The result suggests that the signaling of the Q to L mutant was inhibited by binding of SHP-1.

4. Discussion

In this study, we employed an approach to engineer a tyrosine motif located at the intracellular domain of a cytokine receptor. Consequently, we attained the enhanced proliferation level of HSCs in vitro through the signaling of the S-Mpl mutant, "trunc.". There are two major approaches to the motif engineering of cytokine receptors; the bottom-up and top-down approaches. In the bottom-up approach which we recently developed, tyrosine motifs are artificially fused downstream of the JAK binding domain of c-Mpl (Saka et al., 2013, 2012). The tyrosine motifs consist of approximately 10 amino-acid residues which include one tyrosine residue in the center. Our constructed chimeric receptor incorporating such a tyrosine motif can preferentially activate the corresponding signaling molecule. This bottom-up approach has several advantages. First, since these motifs provide only the minimal essential site to recruit a signaling molecule of interest, unintended signaling pathways are rarely activated compared with wild-type receptors and amino-acid substitution mutants that have various tyrosine motifs. Second, such artificial receptors could be a valuable tool for specific activation of target signaling molecules, which could be further applied to investigate the role of the signaling molecules in controlling cellular fates. However, this approach might have potential difficulty in reconstituting highly synergistic nature of endogenous signaling events from scratch, which may limit practical applications.

The top-down approach is based on the engineering of the receptor intracellular domains through substitution or truncation. Previous studies showed that the signaling pattern could be changed by top-down construction of receptors, such as introducing mutations in the intracellular domain (Gurney et al., 1995; Levin et al., 1998; van der Geer et al., 1999). However, these previous studies were directed solely for functional analyses of cytokine receptors, but not directed for applications such as the development of the method to efficiently control cell fates.

Therefore, we aimed to engineer the intracellular domain of a cytokine receptor through the top-down approach for directing ex vivo expansion of HSCs. The truncated mutant, in which the YWQQ motif of S-Mpl is deleted, showed higher activation level of STAT3 and STAT5 than WT. Since the expression level of the truncated mutant was 1.4 times higher than that of WT, the result indicated that the surface expression levels of the chimeric receptors may partially contribute to the increased activation level. Previously, it was reported that epidermal growth factor receptor (EGFR) has a Tyr974-containing internalization motif and interacts with clathrin adaptors (Sorkin et al., 1996). Kazi et al. demonstrated that phosphorylated Tyr591 and Tyr919 of Flt3 bind to suppressor of cytokine signaling 6 (SOCS6). SOCS6 is a negative regulator of Flt3 signaling and enhances ubiquitination of Flt3, as well as internalization and degradation of the receptor (Kazi et al., 2012). The YWQQ motif at the C-terminus of c-Mpl might be involved in such negative regulation of signaling. Moreover, the YWQQ motif at the C-terminus might competitively block the recruitment of

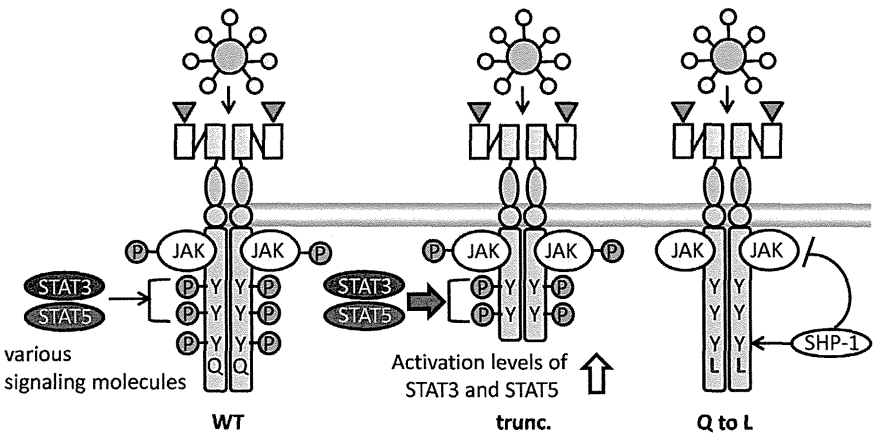

Fig. 7. Our proposed model of signaling through the mutants of S-Mpl.

STAT3 and STAT5 to the adjacent Y^{626}LPL motif (Saka et al., 2013). Our result demonstrated that the truncated mutant induced HSC proliferation more efficiently than WT when stimulated with SCF and BSA-FL. The level of proliferation was higher than that of non-transduced HSCs with the stimulation of SCF and TPO. Thus, the truncated mutant may be useful for the ex vivo expansion of HSCs.

On the other hand, the Q to L mutant, in which the YWQQ motif of S-Mpl was converted into the YWQL motif, transduced virtually no signaling in Ba/F3 cells. This phenomenon is consistent with the result of the HSC proliferation assay. These results indicated the existence of some negative feedback mechanism in the Q to L mutant. Pull-down assay revealed that SHP-1 was found out as one of the negative regulators. It is known that the STAT5 and SHP-1 binding consensus motif sequences are YXXL and I/V/LXYXXL/V (X: any amino acid), respectively (Daeron et al., 2008; Klingmuller et al., 1996). Thus, depending on the surrounding sequence, the YXXL motif may function as SHP-1 binding motif, which would competitively abrogate binding of STAT5. It is most likely the case since the Q to L mutation creates the SHP-1 binding consensus motif (LXYXXL). Therefore, the sequence which surrounds the motif should be carefully determined for the tyrosine motif to recruit target signaling molecules specifically. Taken our findings in this study together, we propose the model for the signaling mechanisms through the S-Mpl mutants (Fig. 7).

Here we engineered the tyrosine motif in the scFv/c-Mpl chimera, and demonstrated that the truncated mutant exerted stronger effect on HSC proliferation. This is the first demonstration that a non-natural artificial mutant of a cytokine receptor is effective for ex vivo expansion of hematopoietic cells. The top-down motif engineering may be applied to efficiently control various cellular fates of other clinically relevant cells.

Acknowledgments

We are grateful to Dr T. Kitamura (The University of Tokyo) for Plat-E cells. This work was supported by Grants-in-Aid for Young Scientists (A) 21686077 (M.K.) and for Challenging Exploratory Research 23656516 (M.K.) from the JSPS, Japan, by the Program for Promotion of Basic and Applied Researches for Innovations in Bio-oriented Industry (BRAIN) (M.K.) and by the Global COE Program for Chemistry Innovation.

References

Abboud, M.R., Xu, F., Payne, A., Laver, J., 1994. Effects of recombinant human steel factor (c-kit ligand) on early cord blood hematopoietic precursors. Exp. Hematol. 22, 388–392.

Burns, J.C., Friedmann, T., Driever, W., Burrascano, M., Yee, J.K., 1993. Vesicular stomatitis virus G glycoprotein pseudotyped retroviral vectors: concentration to very high titer and efficient gene transfer into mammalian and nonmammalian cells. Proc. Natl. Acad. Sci. U.S.A. 90, 8033–8037.

Chung, Y.J., Park, B.B., Kang, Y.J., Kim, T.M., Eaves, C.J., Oh, I.H., 2006. Unique effects of Stat3 on the early phase of hematopoietic stem cell regeneration. Blood 108, 1208–1215.

Daeron, M., Jaeger, S., Du Pasquier, L., Vivier, E., 2008. Immunoreceptor tyrosine-based inhibition motifs: a quest in the past and future. Immunol. Rev. 224, 11–43.

Dahlberg, A., Delaney, C., Bernstein, I.D., 2011. Ex vivo expansion of human hematopoietic stem and progenitor cells. Blood 117, 6083–6090.

Datta, S.R., Dudek, H., Tao, X., Masters, S., Fu, H., Gotoh, Y., Greenberg, M.E., 1997. Akt phosphorylation of BAD couples survival signals to the cell-intrinsic death machinery. Cell 91, 231–241.

Geest, C.R., Coffer, P.J., 2009. MAPK signaling pathways in the regulation of hematopoiesis. J. Leukoc. Biol. 86, 237–250.

Gow, D.J., Garceau, V., Kapetanovic, R., Sester, D.P., Fici, G.J., Shelly, J.A., Wilson, T.L., Hume, D.A., 2012. Cloning and expression of porcine colony stimulating factor-1 (CSF-1) and colony stimulating factor-1 receptor (CSF-1R) and analysis of the species specificity of stimulation by CSF-1 and interleukin 34. Cytokine 60, 793–805.

Gurney, A.L., Wong, S.C., Henzel, W.J., de Sauvage, F.J., 1995. Distinct regions of c-Mpl cytoplasmic domain are coupled to the JAK-STAT signal transduction pathway and Shc phosphorylation. Proc. Natl. Acad. Sci. U.S.A. 92, 5292–5296.

Ihle, J.N., 1995. Cytokine receptor signaling. Nature 377, 591–594.

Ivashkiv, L.B., Hu, X., 2004. Signaling by STATs. Arthritis Res. Ther. 6, 159–168.

Kaneko, E., Kawahara, M., Ueda, H., Nagamune, T., 2012. Growth control of genetically modified cells using an antibody/c-kit chimera. J. Biosci. Bioeng. 113, 641–646.

Kato, Y., Iwama, A., Tadokoro, Y., Shimoda, K., Minoguchi, M., Akira, S., Tanaka, M., Miyajima, A., Kitamura, T., Nakauchi, H., 2005. Selective activation of STAT5 unveils its role in stem cell self-renewal in normal and leukemic hematopoiesis. J. Exp. Med. 202, 169–179.

Kaushansky, K., 2005. The molecular mechanisms that control thrombopoiesis. J. Clin. Invest. 115, 3339–3347.

Kawahara, M., Chen, J., Sogo, T., Teng, J., Otsu, M., Onodera, M., Nakauchi, H., Ueda, H., Nagamune, T., 2011. Growth promotion of genetically modified hematopoietic progenitors using an antibody/c-Mpl chimera. Cytokine 55, 402–408.

Kazi, J.U., Ronnstrand, L., 2012. Src-like adaptor protein (SLAP) binds to the receptor tyrosine kinase Flt3 and modulates receptor stability and downstream signaling. PLoS One 7, e53509.

Kazi, J.U., Sun, J., Phung, B., Zadjali, F., Flores-Morales, A., Ronnstrand, L., 2012. Suppressor of cytokine signaling 6 (SOCS6) negatively regulates Flt3 signal transduction through direct binding to phosphorylated tyrosines 591 and 919 of Flt3. J. Biol. Chem. 287, 36509–36517.

Klingmuller, U., Bergelson, S., Hsiao, J.G., Lodish, H.F., 1996. Multiple tyrosine residues in the cytosolic domain of the erythropoietin receptor promote activation of STAT5. Proc. Natl. Acad. Sci. U.S.A. 93, 8324–8328.

Levin, I., Cohen, J., Supino-Rosin, L., Yoshimura, A., Watowich, S.S., Neumann, D., 1998. Identification of a cytoplasmic motif in the erythropoietin receptor required for receptor internalization. FEBS Lett. 427, 164–170.

Morita, S., Kojima, T., Kitamura, T., 2000. Plat-E: an efficient and stable system for transient packaging of retroviruses. Gene Ther. 7, 1063–1066.

Ohmizono, Y., Sakabe, H., Kimura, T., Tanimukai, S., Matsumura, T., Miyazaki, H., Lyman, S.D., Sonoda, Y., 1997. Thrombopoietin augments ex vivo expansion of human cord blood-derived hematopoietic progenitors in combination with stem cell factor and flt3 ligand. Leukemia 11, 524–530.

Ory, D.S., Neugeboren, B.A., Mulligan, R.C., 1996. A stable human-derived packaging cell line for production of high titer retrovirus/vesicular stomatitis virus G pseudotypes. Proc. Natl. Acad. Sci. U.S.A. 93, 11400–11406.

Osawa, M., Hanada, K., Hamada, H., Nakauchi, H., 1996. Long-term lymphohematopoietic reconstitution by a single CD34-low/negative hematopoietic stem cell. Science 273, 242–245.

Piacibello, W., Sanavio, F., Garetto, L., Severino, A., Dane, A., Gammaitoni, L., Aglietta, M., 1998. The role of c-Mpl ligands in the expansion of cord blood hematopoietic progenitors. Stem Cells 2, 243–248.

Rossi, D.J., Weissman, I.L., 2006. Pten, tumorigenesis, and stem cell self-renewal. Cell 125, 229–231.

Saka, K., Kawahara, M., Nagamune, T., 2013. Reconstitution of a cytokine receptor scaffold utilizing multiple different tyrosine motifs. Biotechnol. Bioeng., doi:10.1002/bit.24973.

Saka, K., Kawahara, M., Ueda, H., Nagamune, T., 2012. Activation of target signal transducers utilizing chimeric receptors with signaling-molecule binding motifs. Biotechnol. Bioeng. 109, 1528–1537.

Salmena, L., Carracedo, A., Pandolfi, P.P., 2008. Tenets of PTEN tumor suppression. Cell 133, 403–414.

Songyang, Z., Shoelson, S.E., Chaudhuri, M., Gish, G., Pawson, T., Haser, W.G., King, F., Roberts, T., Ratnofsky, S., Lechleider, R.J., Neel, B.G., Birge, R.B., Fajardo, J.E., Chou, M.M., Hanafusa, H., Schaffhausen, B., Cantley, L.C., 1993. SH2 domains recognize specific phosphopeptide sequences. Cell 72, 767–778.

Sorkin, A., Mazzotti, M., Sorkina, T., Scotto, L., Beguinot, L., 1996. Epidermal growth factor receptor interaction with clathrin adaptors is mediated by the Tyr974-containing internalization motif. J. Biol. Chem. 271, 13377–13384.

van der Geer, P., Wiley, S., Pawson, T., 1999. Re-engineering the target specificity of the insulin receptor by modification of a PTB domain binding site. Oncogene 18, 3071–3075.

Walasek, M.A., van Os, R., de Haan, G., 2012. Hematopoietic stem cell expansion: challenges and opportunities. Ann. N.Y. Acad. Sci. 1266, 138–150.

Weichhart, T., Saemann, M.D., 2008. The PI3K/Akt/mTOR pathway in innate immune cells: emerging therapeutic applications. Ann. Rheum. Dis. 67, iii70–iii74.